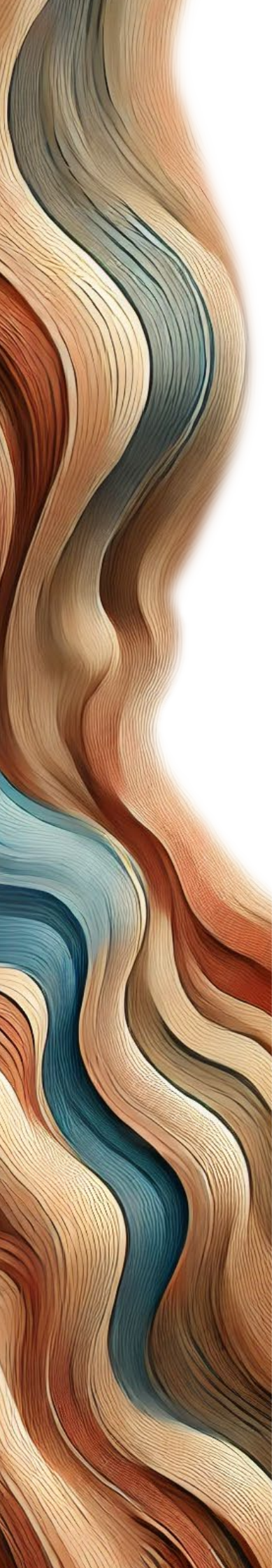

Modelling Tidal Sandbank Dynamics and Impacts of Sand Extraction in Sediment-Scarce Environments

Literature Report

Sem J. Geerts

September 2025

UNIVERSITY OF TWENTE.

Faculty of Engineering Technology
Department of Civil Engineering & Management
Marine and Fluvial Systems

CE&M research report 2025R-003/WEM-003
ISSN 1568-4652

Contents

Contents 1

1 Introduction 3

2 Tidal Sandbanks and the Belgian Continental Shelf 5

2.1 Classification of Tidal Sandbanks . . . 5
2.2 Dynamics of Tidal Sandbanks . . . 6
2.3 The Belgian Continental Shelf . . . 6

3 Governing Physical Processes and Model Formulations 8

3.1 Morphodynamic Modelling Approaches . . . 8
3.2 The Morphodynamic Loop . . . 10
3.3 Hydrodynamics . . . 11
3.4 Sediment Transport . . . 12
3.4.1 The Initiation of Motion . . . 12
3.4.2 Bedload Sediment Transport . . . 12
3.4.3 Suspended Sediment Transport . . . 13
3.4.4 Non-Uniform Sediment: Hiding-Exposure Effect . . . 14
3.5 Bed Evolution . . . 15
3.5.1 Bed Load Transport and the Quasi-Stationary Approach . . . 15
3.5.2 Suspended load . . . 16
3.5.3 Non-Uniform Sediment: Layering . . . 16
3.6 Linear Stability Analysis (LSA) . . . 17
3.7 Influence of Processes on Sandbank Shape and Dynamics . . . 18
3.7.1 Tides: velocity, constituents and ellipticity . . . 18
3.7.2 Bed Friction and Sediment Transport Formulation . . . 19
3.7.3 Sediment Properties . . . 19
3.7.4 Finite Stage Behaviour . . . 19

4 Sand Extraction 22

4.1 Sand Extraction on the Belgian Continental Shelf . . . 22
4.2 Morphodynamic Response to Sand Extraction . . . 22
4.3 Effects of Sand Extraction on Bedforms and Fauna . . . 23

5 Sediment Scarcity 25

5.1 Sand as an Important and Scarce Resource . . . 25
5.2 Sediment Scarcity in the Belgian Continental Shelf . . . 25
5.3 Influence of Sediment Scarcity on Bedforms . . . 26

5.4 Bedload Transport over Non-Erodible Layers 27
5.5 Modelling of Sediment Scarcity 28
5.5.1 Adapting Transport based on Divergence Rule 28
5.5.2 Struiksma Method 28
5.5.3 Limiting Erosion using Suspended Load 28
5.5.4 Iterative Prediction Correction 29
5.5.5 Optimisation Problem 29

6 Conclusions **30**

Bibliography **31**

Chapter 1

Introduction

The North Sea spans the exclusive economic zones of six countries, including the Belgian Continental Shelf (BCS). Sandbanks occur in patches throughout the North Sea as shown in Figure 1.1; the Dutch Banks and Zeeland Banks on the NCS, the Flemish Banks on the BCS, and the Norfolk Banks on the British Continental Shelf (Knaapen, 2009). The water depth over a sandbank varies significantly, ranging from 5 m on the crest to 50 m in the trough. These sandbanks provide nursery grounds for fish, sea mammals (Atalah et al., 2013), and macrobenthic species (Wyns et al., 2021). Due to their ecological value, the Flemish Banks are designated as a European Natura 2000 area.

The sediment in the North Sea is mostly composed of sand, clay, and gravel. The thickness of the sand layer varies significantly over the North Sea. The total amount of sand on the BCS is limited and depleting (Van Lancker et al., 2019). Most of the sand that is available in this sediment-scarce system is located in tidal sandbanks. The underlying clay layer is exposed in the troughs between the banks, often together with gravel. Similar characteristics apply to the Norfolk Banks on the British Continental Shelf, where coarse sediment is found in the troughs (Caston, 1972).

Marine sand is needed for coastal nourishments, land reclamation and the construction industry (Torres et al., 2021). Due to their shallow water depth on the crest, sandbanks form attractive locations for sand extraction (Degrendele et al., 2010; Van Lancker et al., 2010b, 2010a). Consequently, a significant portion of the total mined sand is extracted from sandbanks, such as the Noordhinder, Thornton and Kwinte Banks (Degrendele et al., 2010; Wyns et al., 2021). The morphodynamic response to sand extractions from sandbanks in a sediment-scarce environment is unknown. However, it may threaten the morphological balance of the environment with adverse impacts on future sand stocks, sediment quality, foundations of wind farms, protected Natura 2000 areas and associated marine flora and fauna (Wyns et al., 2021; Van Lancker et al., 2022).

In view of the above, the NWO-funded BANX project aims to develop more sustainable sand extraction strategies and safeguard valuable resources and habitats for future generations. Specifically, it aims to

Understand Tidal Sandbank Dynamics and the Influence of Sand Extraction in Sediment-Scarce Environments

This literature report serves three purposes: (i) providing an overview of the existing knowledge surrounding tidal sandbank dynamics within the BANX context, (ii) identifying knowledge gaps, and (iii) examining existing modelling strategies. To this end, the following literature questions will be answered:

Q1 What are tidal sandbanks and what is their relation to the Belgian Continental Shelf?

Q2 What are the governing physical processes of tidal sandbank dynamics and how can this be modelled?

Q3 How do large-scale sand extractions influence hydrodynamic and morphodynamic processes?

Q4 How does sediment scarcity influence bedform development and how can this be modelled?

In answering Q1, we mostly focus on the Belgian Continental Shelf and describe the basics of tidal sandbank formation, supported by both field observations and modelling studies. Answering Q2 provides additional detail, reviewing modelling studies and describing the sensitivity of sandbank morphodynamics to modelling choices and physical processes. Q3 examines the influence of sand extraction on tidal sandbank dynamics. Answering Q4 provides the setting of sediment-scarce environments and highlights the influence of sediment scarcity on bedforms and discusses modelling opportunities.

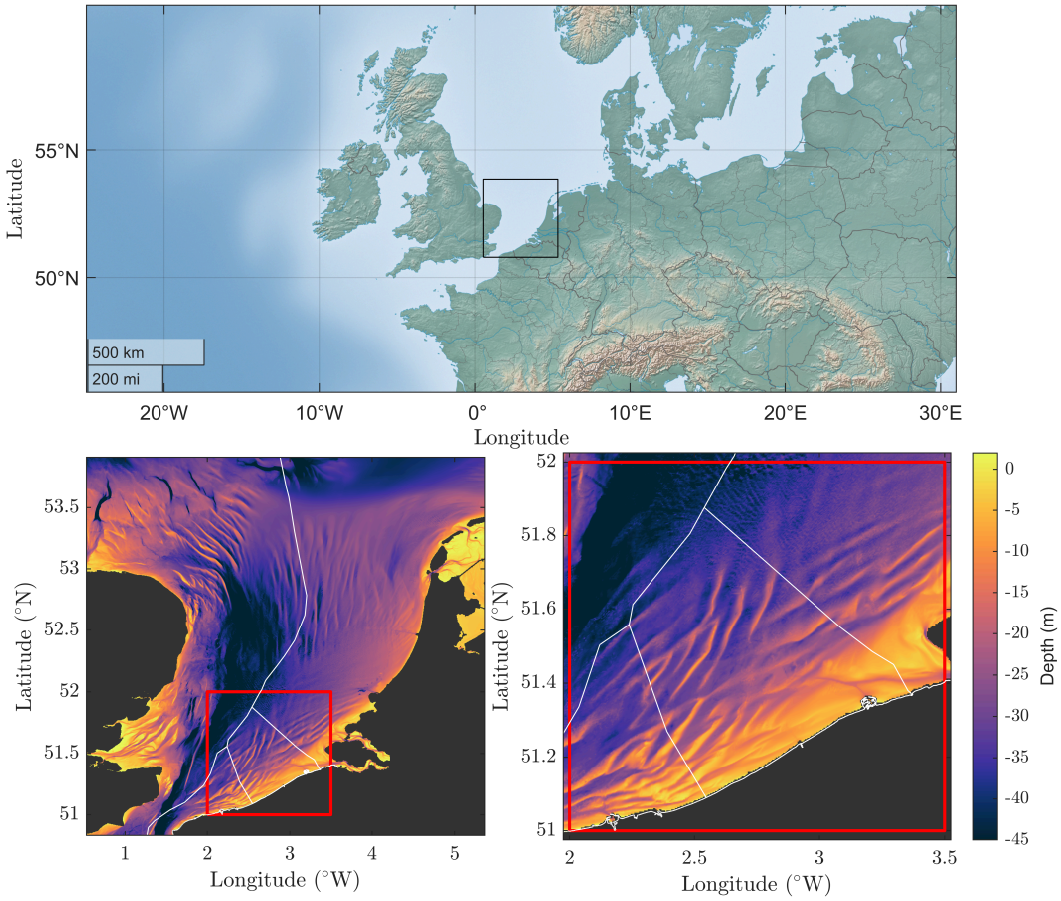

Figure 1.1: Top: location of the Southern North Sea. Bottom two panels further zoom in on the bathymetry of the Southern North Sea. White lines indicate the borders of the Exclusive Economic Zones (EEZ) of the UK, Netherlands, Belgium and France. Bathymetry data is from EMODnet. The highlighted area (red box in the lower panels) shows the Belgian Continental Shelf (or the Belgian EEZ), a system known as a sediment-scarce environment with several tidal sandbanks. The names and zonation of the Belgian tidal sandbanks are shown in Figure 2.1.

Chapter 2

Tidal Sandbanks and the Belgian Continental Shelf

This chapter describes the general properties of tidal sandbanks and how they are formed. We also cover some of the general properties of the Belgian Continental Shelf, illustrating the importance of tidal sandbanks for this region. First, the general concept of sediment transport is introduced, which forms the basis of morphodynamics and bedform evolution. Throughout this research, we will limit ourselves to sand transport only, neglecting the influence of cohesive sediment such as clay.

2.1 Classification of Tidal Sandbanks

In shelf seas with a sandy bed, a variety of rhythmic bedforms patterns can be observed. The crest-to-crest spacing ranges from several centimetres for small ripples to multiple kilometres for the largest structures. In the offshore shelf sea, the largest bedforms are known as tidal sand ridges or tidal sandbanks (de Swart & Yuan, 2019), with heights of 5-30 m, lengths of 5-60 km and crest spacings of 2-15 km (Off, 1963). These bedforms are present in relatively shallow shelf seas with significant tidal flow velocities, such as the North Sea, the Irish Sea and the East China Sea (Off, 1963). Sandbanks evolve over centuries, and their crests are generally cyclonically rotated – counterclockwise in the Northern Hemisphere – to the direction of the principal tidal currents (Caston, 1972), which we refer to as the *bank orientation angle*. Sandbanks are dynamic bedforms; the bathymetry causing a residual depth-averaged (horizontal) flow in anti-cyclonic direction, generating sediment transport patterns that result in their growth and migration (de Swart & Yuan, 2019).

Of similar spatial dimension are shoreface-connected ridges (SFCR), the orientation of which depends on the dominant storm or storm-driven flow direction (Dyer & Huntley, 1999). These ridges are morphodynamically different from offshore ridges, as they are formed by shelf slope and shoreline effects and free surface waves and storm conditions are necessary for their existence (Calvete et al., 2001). This research especially focuses on offshore sand ridges, referred to as tidal sandbanks for the remainder of this report and the specific dynamics of SFCR will not be considered.

Morphologically active sandbanks (de Swart & Yuan, 2019) are present in systems with water depths of approximately 10 to 50 m and sufficiently large (> 0.5 m/s) tidal flow velocities, such as in the Southern North Sea (as shown in Figure 1.1). Moribund sandbanks are morphologically inactive, as waters are too deep (100 to 200 m) and tidal flow velocities are too small. These sandbanks were possibly active in the past, but have "drowned" by sea level rise, becoming inactive (de Swart & Yuan, 2019).

Sand waves are a bedform of smaller scale with heights in the order of metres and wavelengths in the order of tens to hundreds of meters. Similar to tidal sandbanks, they are also formed by the tidal motion, but are governed by subtidal vertical circulation cells. In turn, their crests are aligned orthogonal to the direction of the main flow, and they migrate in the direction of the dominant tidal constituent. Sandbank and sand wave dynamics are believed to be coupled. By shaping the bed on a larger scale, these large sandbanks can interact with smaller bedforms such as sand waves (Caston, 1972; Deleu et al., 2004; Leenders et al., 2021). Conversely, it is hypothesised that sand waves contribute to the growth of tidal sandbanks (Caston, 1972; Komarova & Newell, 2000; Blondeaux et al., 2009).

2.2 Dynamics of Tidal Sandbanks

Several hypotheses have been made regarding the formation mechanism of tidal sandbanks. In this review, we focus on the morphodynamic self-organisation theory, a formation due to a positive feedback loop between water motion and the erodible bed (see Section 3.6) (Dodd et al., 2003). Huthnance (1982) was the first to apply a linear stability analysis to explain the initial formation of tidal sand banks from a flat bed. This yields a fastest growing mode with wavelength and bank orientation angle that agree with field observations. Furthermore, this analysis provides a physical explanation that aligns with the transport patterns observed by Caston (1972), who showed how the dominant sediment transport patterns across the Norfolk banks. On either side of the bank sediment transport is directed in opposing directions, deflected upslope and converging at the crestline. The cross-bank profile is asymmetric, resulting from the dominance of one of the upslope transport streams. In this way, it is believed that sandbanks grow in height and migrate in the direction of the steeper side.

Process-based morphodynamic models show how bed friction and the Coriolis effect together create anti-cyclonically vorticity of the water column, resulting in cyclonically rotated sandbanks relative to the tide (Hulscher et al., 1993; Roos & Hulscher, 2003). This creates larger sediment transport on the upstream slope of the bank, resulting in net sediment transport convergence towards the crest during both ebb and flood. Sandbank growth will eventually saturate, because of the divergence of sand by downslope dispersion and free surface wave-stirring, causing more sediment transport on the crest (Roos et al., 2004). The formation mechanisms and the spatial scale involved mean that these processes all occur on a centennial timescale. Hence, these tidal sandbanks may appear stationary in the timeframe of a measurement campaign, while they are dynamic on a larger timescale.

2.3 The Belgian Continental Shelf

The Belgian Continental Shelf (BCS) is part of Belgium's territorial waters and its Exclusive Economic Zone (EEZ) in the North Sea. The region has a relatively shallow depth of 10 to 40 m, which makes it suitable for economic activities like fisheries, wind farms, and dredging. While the Flemish government manages the coastline and coastal protection, the BCS is managed by the (national) Federal Public Service.

The hydrodynamics are dominated by the M2, S2 and N2 tidal constituents, making it a semi-diurnal system, with amplitudes of approximately 1.7, 0.5 and 0.3 m respectively. Tidal currents are relatively strong due to the small water depth and the narrowing of the North Sea through the Canal. Typical currents range between 0.5 and 1.5 m/s, decreasing in magnitude from Southwest to Northeast.

As visible in Figures 1.1, most of the BCS is covered by tidal sand ridges. Figure 2.1 provides the names for the bank and categorises them in four regions. The Coastal Banks (Kustbanken, in blue) are located in the shallow regions near the coast, ranging from 15 to 0 meters in depth. These also include

shoreface-connected ridges, which are dominated by wind-driven currents and sediment transport and feed sediment to the coast (Dujardin et al., 2023; Geerts et al., 2023; Verwaest et al., 2024). Two of these ridges (Stroombank and Wenduine - Paardemarkt system) are disturbed by maintenance dredging activities of entrance channels to the Oostende and Brugge seaports. The Zeeland Banks (in yellow) are part of a bigger construct that continues further on the Dutch continental shelf. The Flemish Banks (Vlaamse banken, in red) are located at depths of 15 to 25 meters. Finally, the Hinder Banks (in yellow) are the banks further offshore with mean depths of 25 to 40 meters.

Whereas the Hinder banks and Flemish banks are considered to be accumulations of sediment due to the self-organisation theory, some of the Zeeland Banks have a resistant core of older deposits, indicating that they are partly erosional remnants (Eisma et al., 1979). Although the Flemish and Hinder banks have an asymmetric cross-sectional shape, they are mostly stationary, having changed little in 300 years (Eisma et al., 1979). In other systems, such as the Coastal banks and the Norfolk banks off the British coast, migration in the order of meters per year is observed (Idier & Astruc, 2003; Dujardin et al., 2023).

In the offshore area, the top Holocene sediment layer comprises mostly coarser sediment types, with mostly medium to coarse sand concentrated in the sandbanks (Hademenos et al., 2019). The crests of the sand banks are composed mostly of medium sand, whereas most coarse sand is located on both the stoss and lee slopes (Kint et al., 2023). Sediment extraction often takes place from sandbanks in all three offshore bank systems. The coastal banks are not used for sand aggregation (anymore), but are still influenced by channel maintenance dredging and the placing of cables and pipelines. The Kwinte bank is an example of a heavily dredged bank, and recent research has focused on investigating the morphodynamic response. This will be further examined in Chapter 4.

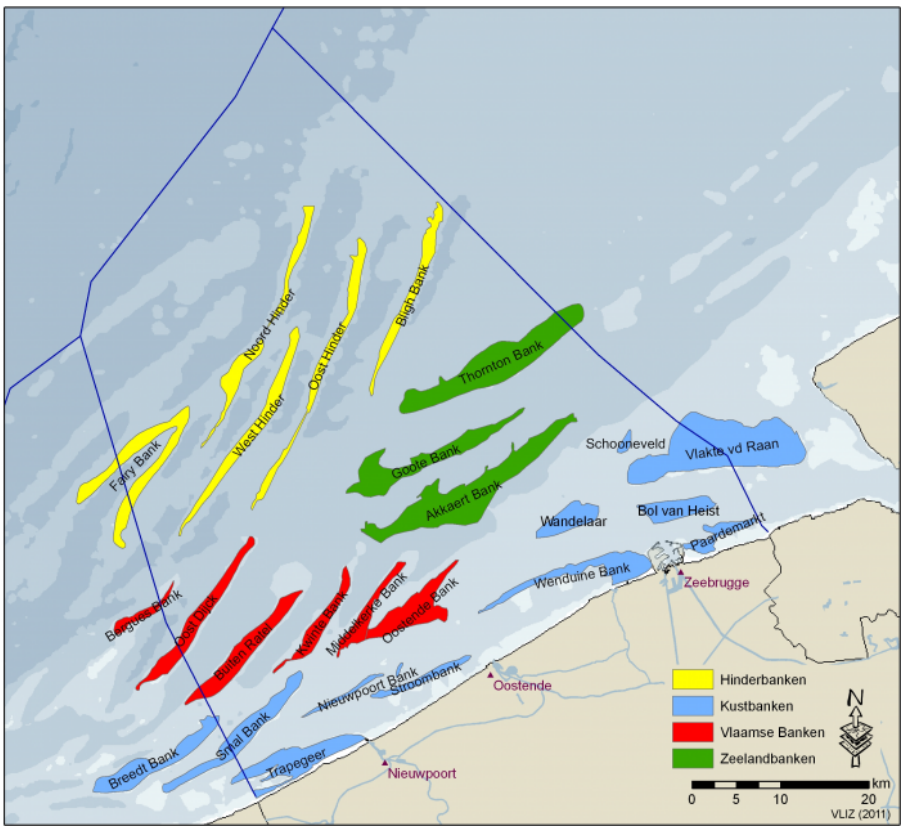

Figure 2.1: Map of the Belgian Continental Shelf with the names of the tidal sandbanks and groupings into the Hinderbanks, Coastal banks, Flemish banks and Zeeland banks (De Hauwere, 2023).

Chapter 3

Governing Physical Processes and Model Formulations

This chapter describes the governing physical processes of tidal sandbanks, specifically focusing on hydrodynamics, sediment transport, and the influence of physical characteristics on the long-term development of tidal sandbanks. We start with a general description of modelling approaches in Section 3.1. Next, the general morphodynamic model set-up used for tidal sandbanks is described using the morphodynamic loop is explained in Section 3.2, of which individual steps are described in Sections 3.3 to 3.4. Section 3.6 describes linear stability analysis in more detail, a specific type of analysis that allows to determine the growth or decay of bedforms. Finally, Section 3.7 describes how different processes shape tidal sandbanks according to these models.

3.1 Morphodynamic Modelling Approaches

Due to the associated timescale, no experimental data and relatively little observational data are available. Therefore, this chapter mostly focuses on the outcomes of process-based morphodynamic models, and we discuss the different types of these kinds of models first:

Complex numerical models simulate morphodynamic processes by discretising space and time into a numerical grid. They solve governing conservation equations[1] along with suitable boundary conditions. These models require careful calibration and validation, along with high computational power. Simulation time is often long. They can be applied to site-specific cases as well as simplified geometries. While their complexity allows for high accuracy and the inclusion of many processes, it also makes them computationally intensive and challenging to interpret due to the multitude of interacting processes. It is generally difficult to run many simulations and clearly dissect the dominating processes and sensitivities.

Idealised models use reduced equations or conceptual approaches to simplify hydrodynamic and morphodynamic processes, allowing isolation of key mechanisms. Usually, this also requires a schematised geometry. These models aim to understand fundamental dynamics rather than replicate specific real-world systems. They are computationally more efficient, making them suitable for large sensitivity analyses and hypothesis testing. However, their assumptions and abstractions limit their ability to capture the full complexity of real-world systems. Within this category, we can distinguish two types:

[1] Conservation equations describe how a certain quantity, such as mass, momentum and energy, is conserved over space and time.

Linear [2] idealised models focus on the initial (linear) response of the physical system after a small perturbation to the bed is applied, also known as a *linear stability analysis*. Here, the morphodynamic stability of each small bed perturbation can be determined, of which the *fastest growing mode* is the perturbation that is most likely to develop initially. This does not allow for modelling the finite-stage behaviour of bedforms where non-linear interactions become more important. Still, this is often a good estimation of the most likely patterns that form, and highlights the sensitivity to physical parameters (Dodd et al., 2003). This method is further examined in Section 3.6 and results are discussed in Section 3.7.

Non-linear idealised models allow us to model the finite-amplitude behaviour of the idealised model equations, either by temporal integration models or by non-linear equilibrium-seeking models. It can be used to predict bedform shapes in morphodynamic equilibrium and the stability of bedforms under temporally varying conditions.

As we are mainly interested in the fundamental mechanisms in the finite-amplitude behaviour of tidal sandbanks from which sediment can be extracted, the focus lies on non-linear idealised models. Linear models can determine the governing processes and sensitivities to these different physical characteristics. However, non-linear evolution models are required to model sand extraction and the influence of sediment scarcity. These involve processes where a well-developed bank is necessary and the initial linear response is not sufficient to capture all processes.

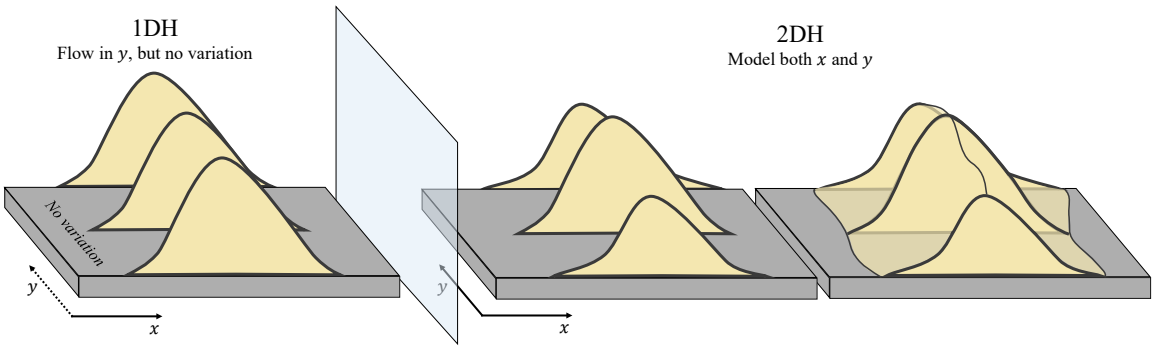

Figure 3.1: Schematisation of 1DH and 2DH sandbank models. Left: assuming little variation in along-crest direction y, motivating the use of a 1DH model that only models cross-sectional variation in direction x. Right: significant variation in cross-sectional shape and physical variables in the along-crest direction y-direction, leading to 2DH model.

For tidal sandbanks, the depth-averaged shallow water equations are usually sufficient to model their morphodynamic evolution towards an equilibrium (e.g. Yuan et al., 2017; Van Veelen et al., 2018; Nnafie et al., 2023), referred to as 2DH models for both horizontal directions[3]. As can be seen in Figure 2.1, the cross-sectional width of tidal sandbanks is usually small compared to the crest length. This is especially true for the Hinderbanks further offshore, and not limited to the BCS (Off, 1963; Caston, 1972; Dyer & Huntley, 1999). Therefore, many model studies have assumed that the flow, free surface elevation and morphodynamics change relatively little in the along-crest direction y. These models do allow the flow component in this along-crest direction, but assume that any change is small ($\partial/\partial y = 0$) compared to the change in across-crest direction x. We refer to these cross-sectional models as 1DH models, which are still capable of producing realistic cross-sectional profiles (e.g. Roos et al., 2004; Van Veelen et al., 2024). Both cases are visualised in Figure 3.1. The main benefit of using a 1DH

[2]Here, by linear we refer to a small perturbation of the bed amplitude, such that the analysis can solely focus on the response of this linear perturbation, analogous to the linear component of a Taylor series. See Section 3.6.

[3]Contrary to 2DV models, which also models two directions, but now including one horizontal and one vertical direction.

model compared to 2DH is the significantly shorter computation time associated with the reduction in model dimension, which allows for covering a wide range of parameter values in a sensitivity analysis more efficiently.

3.2 The Morphodynamic Loop

Morphodynamic models rely on the morphodynamic loop, which forms the structure of the upcoming sections. It is visualised thrice in Figure 3.2 with increasing complexity from left to right. The most basic form is shown on the left; first, an initial bathymetry is required that allows to solve the hydrodynamics over this bathymetry (Section 3.3). The flow solution results in sediment transport formulation (Section 3.4), which in turn results in evolution of the bed (Section 3.5), which defines a new bathymetry for which the loop repeats itself.

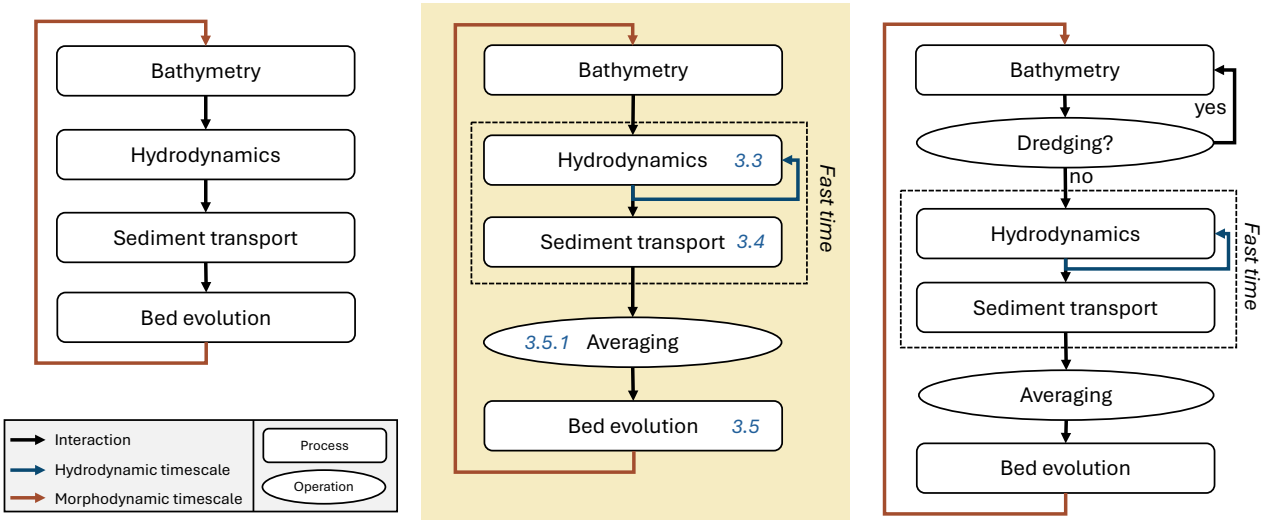

Figure 3.2: Overview of the morphodynamic loop with increasing complexity

On the spatial scale of a tidal sandbank, the changes in bathymetry are relatively small over a tidal cycle. The hydrodynamic changes through a tidal cycle are mostly a consequence of overall bathymetry (large-scale spatial structures) and the tidal forcing: the influence of small temporal changes in bathymetry can be neglected. This is especially true for sandbanks; large spatial structures with long morphodynamic timescales. Hence, these two processes can be decoupled. In practice, this means that the hydrodynamics are solved throughout the tidal cycle with a fixed bed, and only the tide-averaged sediment transport rates are used to update the bed. This is explained in more detail in Section 3.5.1. This methodology is visualised by the *averaging* operation in the middle of Figure 3.2. We refer to this method as the quasi-stationary approach, where the bed is fixed to model on the hydrodynamic timescale (in this case hours), and let the bed evolve over the morphodynamic timescale (years to decades). Note that this method is only valid if these timescales are well apart, and cannot be applied to smaller (read: faster) bedforms. In case of multiple tidal constituents, such as an M2 and S2 tide, this averaging can also be performed over a spring-neap cycle, as long as the morphodynamic timescale is significantly larger than the hydrodynamic timescale used for averaging.

As a last addition to this morphological loop, marine sand extraction can be added. An example of such an implementation is visualised on the right of Figure 3.2, where this occurs after a new bathymetry is defined, after which a new hydrodynamic solution over this bathymetry has to be found again. For computational purposes, other implementations might be possible, such as a gradual implementation of the sand extraction pit. However, we will not cover these different options here.

3.3 Hydrodynamics

Hydrodynamic modelling refers to the study of flow of fluid using mathematical equations. These are usually conservation equations, such as the physical conservation of mass, momentum and energy, supplemented with appropriate boundary conditions. The basis of this is formed by the Navier-Stokes equations. When modelling tidal sandbanks on the continental shelf, several assumptions are usually applied in idealised modelling. This means the flow is (usually) described by the two-dimensional depth-averaged shallow water equations (SWE), which assumes that depth-averaged flow velocities are sufficient to capture the processes related to tidal sandbank formation. In these model equations, the following assumptions are (often) applied

- **No baroclinic pressure gradients:** Density ρ is assumed to be constant and no buoyancy forces apply from temperature or salinity gradients.
- **Shallow water approximation:** The horizontal scales are much larger than the vertical scales, meaning that the vertical momentum equation reduces to the hydrostatic balance.
- **f-plane approximation:** The Coriolis parameter $f = 2\Omega\sin(\varphi)$ (where $\Omega = 7.292 \cdot 10^{-5}$ rad/s is Earth's angular velocity) is assumed to be constant for the modelled region, which is valid when the latitude φ does not vary greatly over the modelled region.

Multiple formulations of the SWE exist, depending on the used numerical method, coordinate system and degree of idealisation. A commonly used non-dimensional system of equations is

$$\frac{\partial h}{\partial t} + \frac{\partial (hu)}{\partial x} + \frac{\partial (hv)}{\partial y} = 0 \tag{3.1}$$

$$\frac{\partial u}{\partial t} + u\frac{\partial u}{\partial x} + v\frac{\partial u}{\partial y} - fv + \frac{\tau_{\mathrm{b},x}}{h} = P_x - g\frac{\partial \zeta}{\partial x} \tag{3.2}$$

$$\frac{\partial v}{\partial t} + u\frac{\partial v}{\partial x} + v\frac{\partial v}{\partial y} + fu + \frac{\tau_{\mathrm{b},y}}{h} = P_y - g\frac{\partial \zeta}{\partial y} \tag{3.3}$$

that describes the mass conservation and momentum conservation in both horizontal directions, respectively. Here, $\boldsymbol{u} = (u, v)$ denotes the depth-averaged horizontal flow vector with components u and v in $\boldsymbol{x} = (x, y)$ direction, and $h = \zeta - z_{\mathrm{b}}$ the local water depth from the free surface elevation $z = \zeta$ (with spatial mean at reference $z = 0$) to the bed $z = z_{\mathrm{b}}$. When modelling tidal sandbanks, the system has a characteristic tidal velocity amplitude U of around 1 m/s and a mean depth H ranging from 20 to 40 m.

Bed friction depends on the local depth-averaged flow velocity and is modelled by the bed shear stress $(\tau_{\mathrm{b},x}, \tau_{\mathrm{b},y})$. The system is forced by $(P_x, P_y)(t)$, a spatially uniform yet temporally-varying barotropic pressure gradient that models the temporal variation by the tide. Parameters f and g denote the (constant) Coriolis parameter and gravitational acceleration, respectively.

The bed shear stress $\boldsymbol{\tau}_{\mathrm{b}} = (\tau_{\mathrm{b},x}, \tau_{\mathrm{b},y})$ is quadratically related to the depth-averaged flow velocity, and can also be linearised by

$$\frac{\boldsymbol{\tau}_{\mathrm{b}}}{\rho} = c_D|\boldsymbol{u}|\boldsymbol{u}. \tag{3.4}$$

with dimensionless friction coefficient c_D. In idealised models, the non-linear form can often increase the computational complexity. In turn, this relation is simplified (idealised) by using the Lorentz' linearisation (Zimmerman, 1982). Here, bed shear stress is described linearly with $\frac{\boldsymbol{\tau}_{\mathrm{b}}}{\rho} = r\boldsymbol{u}$ using $r = \frac{8c_D}{3\pi}U$, for . The value of r ensures that the tidally averaged work done by bed friction is equal for both formulations for a single M2 tide. We refer to the two formulations of Equation (3.4) as the quadratic and linear bed friction formulations, respectively.

Using non-dimensionalisation, the equations above can be simplified further by the **rigid lid approximation**, which is valid when the Froude number $\mathrm{Fr} = U/\sqrt{gH}$ is significantly small ($\ll 1$). In that case, the influence of the free surface elevation ζ on the total water depth $h = \zeta - z_\mathrm{b} \approx -z_\mathrm{b}$ is neglected, and the influence of ζ only remains as a barotropic pressure gradient in Equations (3.2) and (3.3).

3.4 Sediment Transport

A sediment transport formulation describes the local sediment flux $\boldsymbol{q}$ (in m^2/s) and is necessary to close the morphodynamic loop. Sediment transport can occur as bed load, wash load, or as suspended load (or a combination of them), depending on the size of the bed material particles and the flow conditions. We neglect wash load as it does not contribute to the changing bathymetry (Fredsoe & Deigaard, 1992). Sediment transport is often split into different processes depending on the specific grain size. In this case, we consider bedload and suspended load. In this section, we describe these processes separately and how they can be modelled.

3.4.1 The Initiation of Motion

Sediment can be transported by the flow, but only when the flow is strong enough. The movement of a particle will occur when the instantaneous hydrodynamic force is just larger than the instantaneous resisting force by gravity. This resisting force is related to the submerged particle weight and the friction coefficient. In steady flow, the dimensionless bed-shear stress (also known as the Shields stress) is given by

$$\theta = \frac{|\boldsymbol{\tau}_\mathrm{b}|}{(\rho_\mathrm{s} - \rho) g d_\mathrm{m}} \tag{3.5}$$

for the sediment density ρ_s, water density ρ, gravitational acceleration g and median grain diameter d_m. Sand transport occurs when $\theta > \theta_\mathrm{cr}$ for some critical Shields stress θ_cr, which is usually written as a function of the grain Reynolds number

$$\mathrm{Re} = \frac{u_*}{\nu D_{50}} \tag{3.6}$$

Here, ν denotes the kinematic viscosity and $u_* = \sqrt{|\boldsymbol{\tau}_\mathrm{b}|/\rho}$ the shear velocity. If sediment is brought into motion by a sufficiently large bed shear stress, it can be transported by a bedload transport flux $\boldsymbol{q}_\mathrm{b}$ or by suspended transport.

3.4.2 Bedload Sediment Transport

Bedload transport refers to sediment that is being transported while in contact with the bed, or just above by rolling, sliding, and saltating (hopping, but close to the bed). Usually, it is the dominant transport mechanism for sandbanks (Roos et al., 2004; Besio et al., 2006). Several theoretical and (semi-)empirical equations exist to model this process quantitatively. Idealised models often rely on theoretical transport equations that implement several physical processes, resulting in slightly different notation that can not all be combined into one generalised sediment transport equation for mathematical rigour. Using a standardised transport notation does not improve readability; for this, we refer the reader to Amoudry and Souza (2011) and Ploeg (2024) for a review and generalisation. Instead, we introduce and focus on the generalised formulation proposed by Fredsoe and Deigaard (1992) and

extended by Tambroni and Blondeaux (2008):

$$\boldsymbol{q}_\mathrm{b} = \underbrace{\alpha_b(|\boldsymbol{\tau}_b| - \tau_c)\left(\sqrt{|\boldsymbol{\tau}_b|} - \sqrt{\tau_c/2}\right)}_{\text{Magnitude (IV)}} \underbrace{\left(\overbrace{\frac{\boldsymbol{\tau}_b}{|\boldsymbol{\tau}_b|}}^{\text{I}} - \overbrace{G\nabla z_\mathrm{b}}^{\text{II}}\right)}_{\text{Directional}} \overbrace{\mathcal{H}(|\boldsymbol{\tau}_b| - \tau_c)}^{\text{III}}. \tag{3.7}$$

Note that, strictly speaking, the directional component also contains a magnitude due to the addition of two processes (I and II below). In this formulation, we identify the following features that can be incorporated:

I In the absence of a slope, **sediment transport is in the direction of the bed shear stress**, which is also in the same direction of the (depth-averaged) current.

II **Transport moves more easily downhill than uphill.** This is implemented by the proportionality to ∇z_b. The dimensionless tensor G determines whether this is isotropic or anisotropic (relative to the bed shear stress). Usually, isotropic slope-induced transport is modelled, using $G = \lambda I$ for 2×2 identity matrix I and bed-slope coefficient λ, which may be grain size-dependent due to the repose angle of sediment (Idier et al., 2009). Models that use an-isotropicity (e.g. Yuan et al., 2016) take the direction of the bottom stress relative to the bed slope into account. In that case, slope-induced transport is still downhill, but the effect is stronger if the bed shear stress is aligned with this direction of strongest gradient.

III **Sediment only moves when a critical threshold is exceeded,** see Section 3.4.1. The initiation of motion relies on the Shields number. Using Equation (3.5) and the model formulation for bed shear stress $\boldsymbol{\tau}_\mathrm{b}$, this can be written as a function of depth-averaged flow speed $|\boldsymbol{u}|$ so that a critical velocity u_c is defined. In the transport equation, this is modelled by the proportionality using Heaviside function $\mathcal{H}$.

IV From theoretical dimensional analysis and experiments, it was found that the **magnitude of bedload sediment transport scales with** $|\boldsymbol{q}_\mathrm{b}| \propto |\boldsymbol{\tau}_\mathrm{b}|^{\beta/2} \propto |\boldsymbol{u}|^\beta$ where $\beta \approx 3$. Although slightly different power relations are used throughout literature, a cubic relation to the velocity is most common. The exact magnitude used, as controlled by α_b in Equation (3.7) depends on the type of sediment, i.e. relative mass, friction coefficient, grain size and grain shape. We will revisit the influence of heterogeneous sediment (multiple grain sizes) in Section 3.4.4.

V **Wave stirring increase sediment transport.** Surface waves cause additional currents and turbulence, which increases sediment transport. This effect is stronger in shallower water, so inversely proportional to the depth. Instead of the bed shear stress purely by tide-induced velocities alone, sometimes an effective velocity $\boldsymbol{u}_e$ is used to determine the bed shear stress $|\tau_\mathrm{b}| = c_D u_e^2$ that also takes into account. In that case, it is modelled by

$$u_e^2 = |\boldsymbol{u}|^2 + \frac{1}{2}u_w^2, \quad \text{where } u_w = U_w\frac{h}{H}$$

See Roos et al. (2004) and Yuan et al. (2017) for examples of how this can be implemented in the full bedload formulation.

3.4.3 Suspended Sediment Transport

Bedload is the dominant transport mechanism for tidal sandbanks, but suspended sediment can influence the shape of the final sandbank (Roos et al., 2004). Sediment can be picked up and brought into suspension when flow velocities are sufficiently large to pick up (usually smaller) sediment particles. Usually, this suspended sediment transport is modelled by an advection-diffusion equation. For the

depth-averaged SWE, this results in

$$\frac{\partial c}{\partial t} + \frac{\partial (cu)}{\partial x} + \frac{\partial (cv)}{\partial y} = \gamma (c_e - c) + \frac{\partial}{\partial x}\left(K_\mathrm{h} \frac{\partial c}{\partial x} \right) + \frac{\partial}{\partial y}\left(K_\mathrm{h} \frac{\partial c}{\partial y} \right) \tag{3.8}$$

for depth-integrated concentration c and horizontal diffusion coefficient K_h. Horizontal diffusion of suspended sediment is smaller than advection and is often neglected (e.g. Roos et al., 2004; Van Veelen et al., 2024). The entrainment from the bed is modelled with entrainment concentration c_e, depending on the local flow velocity, often defined by

$$c_e = \alpha_\mathrm{s}(u^2 + v^2)$$

as introduced by Schuttelaars and De Swart (1996) and implemented by Roos et al. (2004) for tidal sandbanks. The proportionality constant γ, depending on the fall velocity and vertical diffusion coefficient (Schuttelaars & De Swart, 1996). Together, this results in the production term $\gamma(c_e - c)$. How suspended sediment transport results in a changing bed level is described in Section 3.5.2.

3.4.4 Non-Uniform Sediment: Hiding-Exposure Effect

Most sediment transport formulations quantify the magnitude α_b based on a median grain diameter d_{50}, or assume the sediment to be relatively uniform. In reality, the sediment grain sizes d in a mixture show a large spread. This distribution is usually described using the phi scale, where

$$\phi_d = -\log_2(d/d_\mathrm{ref}), \text{ with } d_\mathrm{ref} = 1 \text{ mm}$$

follows a normal distribution (Dyer, 1986). With multiple sediment fractions and sizes, sediment transport processes change. For example, smaller grain sizes might be transported (mostly) by suspended load, whereas rougher sediment is transported by bedload only.

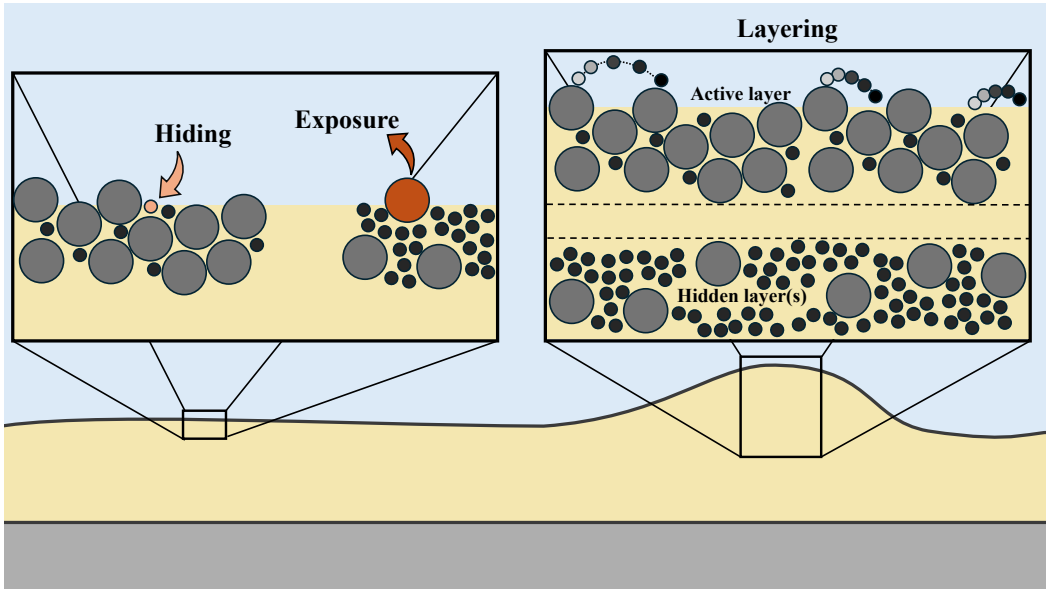

Figure 3.3: Schematisation of two processes involved with multi-model sediment mixtures; hiding-exposure effects (left) and layering (right).

These different sediment sizes also interact and influence each other's transport. An example is the hiding-exposure effect, when there are several (distinct) grain size classes, visualised in Figure 3.3. When a sediment grain size of a given fraction is smaller than the mean grain size d_m, it tends to hide

between larger particles and sediment transport of that given fraction decreases. Conversely, when sediment is significantly larger than the mean sediment diameter, it tends to "stick out" above the bed and gets picked up more easily. This hiding-exposure effect changes the threshold of motion τ_c for each grain fraction, relative to the overall grain size distribution (Ribberink, 1987; McCarron et al., 2019). Several model formulations for this mechanism exist, which usually discretise the continuous sediment size distribution into a discrete distribution of several representative grain size classes. Subsequently, the critical shear stress τ_c is changed based on the ratio of the grain size of a specific fraction $d^{(j)}$ to the median grain size d_{50}.

This mechanism can also be idealised further if no critical shear stress formulation is used in the bedload transport formulation. An example can be found in Roos et al. (2007), who apply this method to study the effect of bimodal sediment distribution on the tidal sandbanks, based on Walgreen et al. (2003). They assume that the overall sediment distribution can be described by a finite number J of sediment fractions $F^{(j)}$ such that $\sum_{j=1}^{J} F^{(j)} = 1$. The total amount of sediment transport is the sum of all contributions $\boldsymbol{q}_\mathrm{b}^{(j)}$, i.e. by

$$\boldsymbol{q}_\mathrm{b} = \sum_{j=1}^{J} \boldsymbol{q}_\mathrm{b}^{(j)} = \sum_{j=1}^{J} F^{(j)} G^{(j)} \boldsymbol{q}_\mathrm{b}^{\mathrm{ref}}.$$

Here, $\boldsymbol{q}_\mathrm{b}^{\mathrm{ref}}$ denotes the reference bedload transport, corresponding to a uniform sediment with diameter d_m. The hiding exposure is modelled by the parameter

$$G^{(j)} = \left(\frac{d^{(j)}}{d_\mathrm{m}} \right)^{c_\mathrm{b}} \quad \text{for } c_\mathrm{b} = 0.75 > 0.$$

Note that d_m can be determined locally as the sediment distributes, resulting in a dynamic hiding-exposure formulation.

3.5 Bed Evolution

Loosely speaking, when more sediment is entering a certain location than is leaving, deposition occurs, and the bed level increases in height (conversely for erosion). The Exner equation describes this, but when modelling tidal sandbanks using the depth-averaged SWE, it is implemented slightly differently for bedload and suspended load, which we discuss independently.

3.5.1 Bed Load Transport and the Quasi-Stationary Approach

The change in bed level z_b is updated according to the Exner equation

$$(1-p)\frac{\partial z_\mathrm{b}}{\partial t} = -\nabla \cdot \boldsymbol{q}_\mathrm{b} \tag{3.9}$$

for porosity p, which is the concentration of voids in the seabed, typically $p \approx 0.4$. When modelling tidal sandbank dynamics, non-dimensional analysis shows that bed level changes occur over a morphodynamic timescale

$$T_\mathrm{mor} = \frac{(1-p)H}{\sigma \alpha_b U^2} = \mathcal{O}(10-100) \text{ years}, \tag{3.10}$$

that is much larger than the tidal timescale $T_\mathrm{tide} = 1/\sigma = 12.42$ h (in case of M2 tide). Hence, the influence of changes of $\boldsymbol{q}_\mathrm{b}$ over the tide on the bed level is negligible to the overall tidal average $\langle \boldsymbol{q}_\mathrm{b} \rangle$.

We refer the reader for details of the non-dimensionalisation to Van Veelen et al. (2018). To conclude, the Exner equation in non-dimensional variables $\widetilde{\cdot}$ reads

$$\frac{\partial \widetilde{z}_\mathrm{b}}{\partial \tau} = -\widetilde{\nabla} \cdot \langle \widetilde{\boldsymbol{q}}_\mathrm{b} \rangle \tag{3.11}$$

where $\tau = t/T_\mathrm{mor}$ is the non-dimensional (morphodynamic) time. In modelling practice (see Figure 3.2), this means the bed load transport can be determined throughout the entire tidal cycle, be averaged, and update the bed level with a much larger time-step, decreasing computational cost.

3.5.2 Suspended load

Most bed evolution equations that rely on a suspended load formulation, as introduced in Section 3.4.3, use a deposition D_s and erosion term E_s in the bed level update

$$(1-p)\frac{\partial z_\mathrm{b}}{\partial t} = D_\mathrm{s} - E_\mathrm{s} \tag{3.12}$$

The used formulation in Equation (3.8) introduces the net production term $D_\mathrm{s} - E_\mathrm{s} = \gamma(c_e - c)$. However, note that the diffusive bed slope mechanism is now implemented, while this is shown to influence suspended load as well (Parker, 1978; Talmon et al., 1995). For a 1DH model, this is implemented by Roos et al. (2004) for tidal sandbanks using the formulation

$$(1-p)\frac{\partial z_\mathrm{b}}{\partial t} = \gamma(c_e - c) - \lambda \frac{\partial}{\partial x}\left(c_e \frac{\partial z_b}{\partial x} \right) \tag{3.13}$$

which, in a 2DH model with non-dimensional variables using the temporal-splitting argument, writes to

$$\frac{\partial \widetilde{z}_\mathrm{b}}{\partial \tau} = \widetilde{\gamma}\langle \widetilde{c}_e - \widetilde{c} \rangle - \widetilde{\lambda}\widetilde{\nabla} \cdot \left(\langle \widetilde{c}_e \rangle \widetilde{\nabla} \widetilde{z}_b \right). \tag{3.14}$$

See again Van Veelen et al. (2024) for the scaling procedure.

3.5.3 Non-Uniform Sediment: Layering

When considering different sediment fractions as introduced in Section 3.4.4, horizontal and vertical (re)distribution of the different grains will occur, known as sorting and layering. In the vertical layering of the system, we distinguish between an exposed *active* layer and underlying deeper layers. Only the sediment available in the active layer can be transported (Walgreen et al., 2003; Roos et al., 2007), and the sediment transport rate is determined for each sediment class independently using an active local hiding-exposure formulation.

When modelling the finite amplitude behaviour of tidal sandbanks over large timescales, the active layer at the top of the seabed subject to transport is not necessarily similar to the (hidden) layers (see Figure 3.3). Hence, the administration of the local layering of the different sediment fractions must be considered. This has been done in a complex numerical model for tidal sandwaves by Damveld et al. (2020). We refer the reader to Ploeg (2024) for an overview.

Inside the active layer, the sediment transport rate $\boldsymbol{q}_\mathrm{b}^{(j)}$ is determined for every sediment class j. Note that (assuming bed-load only) the total Exner equation now reads

$$(1-p)\frac{\partial z_\mathrm{b}}{\partial t} = -\nabla \cdot \left[\sum_{j=1}^{J} \boldsymbol{q}_\mathrm{b}^{(j)} \right]. \tag{3.15}$$

which can be solved to update the bed. Still, the new fraction of each sediment class needs to be known as well. Note that the Exner equation for each sediment class equals (Walgreen et al., 2003)

$$(1-p)\left[F^{(j)}\frac{\partial z_b}{\partial t}+L_a\frac{\partial F^{(j)}}{\partial t}\right]=-\nabla\cdot\boldsymbol{q}_{\mathrm{b}}^{(j)}. \tag{3.16}$$

After multiplication of Equation (3.15) with $F^{(j)}$ and substraction with Equation (3.16), the evolution equation of each fraction $F^{(j)}$ follows:

$$(1-p)L_a\frac{\partial F^{(j)}}{\partial t}=F^{(j)}\nabla\cdot\left[\sum_{j=1}^{J}\boldsymbol{q}_{\mathrm{b}}^{(j)}\right]-\nabla\cdot\boldsymbol{q}_{\mathrm{b}}^{(j)}. \tag{3.17}$$

3.6 Linear Stability Analysis (LSA)

Now that the morphodynamic loop is explained and some equations are highlighted, we introduce one common solving technique to understand the dominant physical processes for morphodynamic responses. Linear stability analysis (LSA), first applied to tidal sandbanks by Huthnance (1982), aims to describe the linear response of a system to a small perturbation. In this section, we go over some basics of this method, as it forms the basis of the next section. For a more general overview, we refer the reader to Dodd et al. (2003).

As a general notation, we introduce the solution vector $\boldsymbol{\phi}$. Although the exact formulation depends on the used model and the processes involved, this solution contains all unknown variables, for example $\boldsymbol{\phi}=(\zeta,u,v,h,\boldsymbol{q}_{\mathrm{b}})$. The basis of this method relies on the assumption that any solution $\boldsymbol{\phi}$ can be written as an expansion of different order terms, analogous to a Taylor expansion:

$$\boldsymbol{\phi}=\boldsymbol{\phi}_0+\epsilon\boldsymbol{\phi}_1+\epsilon^2\boldsymbol{\phi}_2+\mathcal{O}(\epsilon^3), \tag{3.18}$$

for dimensionless expansion parameter $\epsilon<1$, for tidal sandbanks the ratio of bank height to mean water depth. The basic state $\boldsymbol{\phi}_0$ describes a solution of an equilibrium situation, for which usually a flat bed system is used. This equilbrium may be stable, in which case a small perturbation will cause decay of the perturbation, returning back to the basic state. Alternatively, the basic state is an unstable equilibrium, meaning that a small perturbation will cause a dynamic response that causes the perturbation to grow. In LSA, this perturbation is given to bed level, by

$$h=h_0+\epsilon h_1$$

with topographic perturbation h_1 on basic state h_0. As long as ϵ is small, we can neglect the influence of higher-order terms in Equation (3.18). As the basic state $\boldsymbol{\phi}_0$ is known, the perturbation solution $\boldsymbol{\phi}_1$ can be determined for any arbitrary perturbation h_1, by collecting all terms linear in ϵ. By Fourier theory, any perturbation can be written as a sum of sinusoidal perturbations. Hence, to simplify, we can determine the influence of any sinusoidal perturbation with wavenumber $\boldsymbol{k}$, by using

$$h_1=\hat{h}_1(t)e^{i(\boldsymbol{k}\cdot\boldsymbol{x})}+\text{c.c.}$$

where c.c. stands for complex conjugate. The temporal amplitude of this specific mode $\boldsymbol{k}$ is denoted by $\hat{h}_1(t)$. In turn, using the linearised version of the Exner equation, the bed level response can be written by

$$\frac{d\hat{h}_1}{dt}=\omega\hat{h}_1.$$

Here, ω is known as the eigenvalue of the problem for given wavenumber $\boldsymbol{k}$. Here, the real part of the eigenvalue $\mathbb{R}\mathrm{e}(\omega)$ determines the growth rate of the perturbation and the migration rate $c_{\boldsymbol{k}} = -\mathbb{I}\mathrm{m}(\omega)/|\boldsymbol{k}|$ is proportional to the imaginary part. If the $\mathbb{R}\mathrm{e}(\omega) < 0$ for all $\boldsymbol{k}$ then the basic state h_0 is (linearly) stable. On the other hand, if there exists a $\boldsymbol{k}$ for which $\mathbb{R}\mathrm{e}(\omega) > 0$, then the basic state is (linearly) unstable. The perturbation with the largest growth rate is known as the fastest growing mode (FGM), and is assumed to dominate the system after some time. Higher-order flow processes, resulting from flow-topography interaction, become relatively more important as the bed develops. The modelled growth resulting from LSA is only valid for small changes to the basic state; perturbations do not grow infinitely. Still, the FGM is a good predictor of the most dominant wavelength found in nature (see Dodd et al. (2003) for a review).

Idealised *analytical LSA* has been successfully used to describe the formation of sandbanks (Huthnance, 1982), sandwaves (Hulscher, 1996), SFCR (Calvete et al., 2001), the sorting of nonuniform sediment on sandbanks (Roos et al., 2007) and SFCR (Walgreen et al., 2003), the influence benthic organisms (Damveld et al., 2019) and of storms on sandwaves (Campmans et al., 2017) and more.

Lastly, we consider the approach of Yuan et al. (2016) to be a *numerical LSA*. Here, a numerical finite difference model is set up, where the initial response to a small perturbation (to stay in the linear regime) is investigated numerically by evolving the bed for a short duration. This allows to include more complex model formulations, such as a non-linear bed shear stress formulation, multiple tidal constituents, critical bed shear stress and anisotropic slope-induced transport, which is not (always) possible for analytic LSA.

3.7 Influence of Processes on Sandbank Shape and Dynamics

In this section, we describe the influence of both external forcing and model formulations on the morphodynamic response of tidal sandbanks. Sections 3.7.1 to 3.7.3 focus on linear results from LSA, whereas Section 3.7.4 focus on the equilibrium bank shapes.

3.7.1 Tides: velocity, constituents and ellipticity

Firstly, the influence of tidal characteristics on sandbank development. The magnitudes of the governing processes - Coriolis force and bottom friction - are both proportional to the local flow velocity. In turn, this is determined by the background tidal activity and the tide-topography interaction, changing the flow locally.

The LSA proposed by Huthnance (1982) uses the depth-averaged SWE with a symmetrical block flow representing the tides, and these results already gives representative wavelengths and orientation to the dominant tidal flow direction. However, this method did not provide a critical velocity while observational data shows that sandbanks only appear where flow velocities are sufficiently large (> 0.5 m/s) (Off, 1963; Dyer & Huntley, 1999). Hulscher et al. (1993) extended the model of Huthnance (1982) to include a smooth periodic M2 tide, and showed that an elliptical tide (rather than uni-directional) is required to obtain such a velocity threshold.

The numerical LSA of Yuan et al. (2016) results in larger wavelengths and larger orientation angles of the FGM compared to the results of analytical LSA Hulscher et al. (1993). This method shows that a diurnal tidal constituent, a mixed tide with significant diurnal component, and a spring-neap cycle all cause the formation of bedforms with larger wavelengths Yuan et al. (2016). The growth rate remains intact.

3.7.2 Bed Friction and Sediment Transport Formulation

Huthnance (1973) shows with a theoretical model that the linear and quadratic friction laws generate the same mean current and vorticity responsible for the generation of sandbanks. Roos et al. (2008) models the evolution of sand pits using LSA, which morphologically follow the same growth patterns as sand banks, and also find that the qualitative and quantitative behaviour of growth are almost the same for the linear and the quadratic friction parametrization. Quantitatively, using a non-linear bed shear stress increases the growth rate and decreases the wavelength of the FGM. Increasing the bed roughness shortens the wavelength (Roos & Hulscher, 2003).

Similar characteristics hold for the threshold of motion, which does not influence results qualitatively (Hulscher et al., 1993), but does decrease the growth rate, wavelength and orientation angle quantitatively (Yuan et al., 2016).

Huthnance (1982) showed that the downhill transport term (II in Equation (3.7)) is required to suppress the generation of short wavelengths. Idier and Astruc (2003) expand on these processes, showing that the current-driven sediment flux controls the orientation of the FGM, whereas the wavelength is controlled by downslope movement. Similarly, Yuan et al. (2016) anisotropic slope-induced transport both increase the growth rate and decrease the wavelength.

3.7.3 Sediment Properties

Roos et al. (2007) described the influence of a bimodal sediment mixture (including a hiding-exposure formulation) on the morphodynamics of tidal sandbanks. Using LSA, this shows how the two sediment fractions spread over the sandbank. Symmetrical tides result in an accumulation of the coarsest sediment on the crest, whereas asymmetric tides cause accumulation on the lee side. With non-uniform sediment, the growth rates of the perturbations increase. A non-linear finite-stage model describing the spatial distribution of different grain sizes does not exist for tidal sandbanks.

Idier et al. (2009) investigate the influence of the grain size of a uniform sediment on the dynamics and geometrical properties of the sandbank using LSA. In their model, the grain size changes the critical bed shear stress τ_c and the bed slope coefficient λ. In the linear case, the influence of changing λ is negligible. Including the effect of the grain size on the critical bed shear stress changes the predicted geometrical properties of the FGM and improves the sandbank wavelength prediction compared to observations.

3.7.4 Finite Stage Behaviour

Finally, we focus on the influence of model changes or physical parameters in non-linear models, capable of producing the morphodynamic evolution to sandbanks in dynamic equilibrium with the tide. Tidal asymmetry, introduced by multiple high-harmonic (such as M4 together with M2) tidal constituents, causes smoothening of the cross-sectional profile and asymmetry in the profiles (Roos et al., 2004). The influence of tidal ellipticity mainly presents itself in the shape of the sandbanks; the global growth time varies nonmonotonically with the tidal ellipticity (Yuan et al., 2017). With sea level rise (SLR), growth rates decrease, and active sand ridges can become quasi-active due to a decrease in tidal flow velocity (Yuan & de Swart, 2017). This timescale for this to occur is inversely proportional to the rate of SLR.

Furthermore, enabling suspended sediment transport (Section 3.4.3) and increasing wave stirring (V in Section 3.4.2) both smooth the cross-sectional profile. Using a bedload transport formulation with a symmetrical tide results in high and spiky bank crests (Roos et al., 2004). The authors note that fully time-resolving is necessary, using a block-flow and omitting inertia terms does not capture the nonlinear effects required to produce these effects. Equilibrium sandbank shapes are hardly sensitive

to the critical bed shear stress, but the global growth time (time from flat bed to equilibrium) increases if the critical bed shear stress is included (Yuan et al., 2017).

In general, in most non-linear models that evolve towards a sandbank in equilibrium, the bank height is overpredicted compared to field measurements (Idier & Astruc, 2003; Roos et al., 2004; Yuan & de Swart, 2017; Yuan et al., 2017). An overview of all sensitivities described above is provided in Table 3.1.

Table 3.1: Overview of sandbank sensitivities

	Linear response of the FGM				Finite stage behaviour			Sources
Process	Growth	Migration	Wavelength	Angle[a]	Height	Asymmetry	Shape	
Flow velocity	faster				higher			Tambroni and Blondeaux (2008)
Tidal asymmetry		faster	no effect	no effect	smaller	increases	smoothening	Roos et al. (2004)
Tidal ellipticity	slower		longer	non-monotonic	smaller			Yuan et al. (2016) Yuan et al. (2017)
Diurnal tide	no effect		longer	smaller				Yuan et al. (2016)
Spring-neap cycle			longer					Yuan et al. (2016)
Residual flow (M0)		faster	no effect	no effect	smaller	increases		Roos et al. (2004)
Sea level rise					higher			Yuan and de Swart (2017)
Wind wave stirring			no effect	no effect	smaller		smoothening	Roos et al. (2004) Yuan et al. (2017)
Suspended transport			no effect	no effect			smoothening	Roos et al. (2004)
Higher roughness		slower	shorter	smaller	higher		steeper	Yuan et al. (2016) Van Veelen et al. (2024)
Larger grain size	slower		shorter	smaller				Idier et al. (2009)
Higher λ	slower		shorter	larger	smaller			Idier et al. (2009) Roos et al. (2004)
Critical shear	slower		shorter	smaller			no influence	Idier et al. (2009) Yuan et al. (2016) Yuan et al. (2017)
Anisotropic slope term	faster		shorter	no effect				Yuan et al. (2016)
Non-linear[b] τ_b	faster		shorter	larger				Yuan et al. (2016)

[a] The bank orientation angle w.r.t. to the dominant M2 tidal direction

[b] Often a linear bed shear stress formulation is used for analytical purposes. Therefore, while physically more correct, a non-linear bed shear stress is the exception here.

Chapter 4

Sand Extraction

In this chapter we examine the influence of sand extraction on the morphology, hydrodynamic conditions and fauna, specifically on the Belgian Continental Shelf.

4.1 Sand Extraction on the Belgian Continental Shelf

Marine sand extraction from the BCS started in 1976, and for most of the time the maximum extraction depth has been limited to 0.50 m (Van Lancker et al., 2010b). Currently, four extraction sites (control zones) have been appointed (Wyns et al., 2021), concentrated on the crests of the tidal sandbanks (see Figure 4.1), and dredging regulations are location-dependent. Annual extraction volumes are around 3 million m^3 (De Backer et al., 2017), and these extraction rates are increasing (Roche et al., 2017). Extraction takes place from tidal sandbanks where most sand is present, but also because it was previously believed that the sandbanks naturally regenerate and can "heal" (Van Lancker et al., 2010b). However, both field observations and modelling have pointed out that, if even occurring at all, recovery may take longer than expected (Degrendele et al., 2010; Van den Eynde et al., 2010). Furthermore, this assumption relies on the availability of new sand, which is not guaranteed (Chapter 5). Wyns et al. (2021) add that both the extraction regime (comprised of intensity and frequency) and the local geological and sedimentary setting influence the morphological response. For example, some regions show coarsening after extraction, whereas others show fining. Sand extraction pits change the significant wave height locally, but the influence on the wave height at the coast is negligible (Van den Eynde et al., 2019). Still, if the morphological balance is disturbed, the implications for coastal protection may be larger than anticipated.

4.2 Morphodynamic Response to Sand Extraction

There is still relatively little known about the long-term morphological impact of sand extraction. Field measurements primarily show a local response over short timescales (Deleu et al., 2004; Degrendele et al., 2010; Lopez Lopez et al., 2025). However, idealised models show a far greater morphodynamic impact to perturbations over a longer timescale. Blondeaux and Vittori (2005) discuss the evolution of a large-scale sand pit, investigating the effect of the residual current, the tidal asymmetry, the wind waves, and the grain size distribution. They show that the sand pit migrates when a residual current or tidal asymmetry is present, similar to the migration of a sandbank (Roos et al., 2004). The intensity of surface waves does not alter the response qualitatively. This similarity in processes between sandbanks and extraction pits is again shown by Roos et al. (2008), where modelled sandpits trigger the morphodynamic instability associated with the formation of tidal sandbanks, showing deepening,

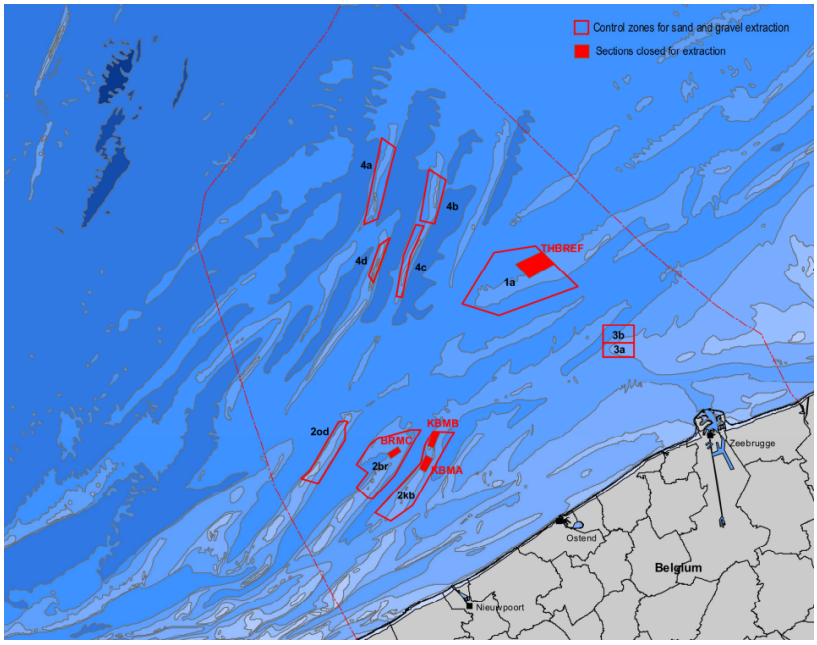

Figure 4.1: Overview of the appointed extraction zones, copied from Durinck and Casteleyn (2017).

deformation and adjacent humps. The morphodynamic response is strongest for sandpits oriented in the direction of the preferred direction of sandbank formation (resulting from LSA), and weakest perpendicular to that direction. In this linear regime, migration only depends on the external flow. González et al. (2010) use a semianalytical numerical model to analyse the morphodynamic evolution of dredged sandpits. They showed that increased wave energy reduces infill time and increases migration, this is increased with lower flow velocities.

The influence of extraction on tidal sandbanks is linked to the stability properties of the equilibrium profile. Relatively little knowledge on this topic is available. Brière et al. (2010) analyse the recovery mechanism of the Kwinte bank using both complex numerical modelling and a long-term idealised modelling approach. No clear recovery pattern is found in the evolution of the depression area based on the complex numerical modelling. However, idealised modelling shows that recovery of an excavated area is expected, resulting in the development of a new sandbank equilibrium during a few centuries.

Using a complex numerical model, Nnafie et al. (2020) investigates the response of sand extraction from tidal sandbanks and finds that the area of morphological influence is significantly larger than the local intervention only. They find that these sandpits and sandbanks recover after a sand extraction on a decadal timescale. The sediment for this recovery is mostly coming from the troughs between the sandbanks and waves aid in the recovery of the sandpits. In this model, when sandpits are deep ($>$ 4 m), the tidal sandbank initially loses sand for 10 years before recovery of the sandbank is initiated. However, these recovery mechanisms for sediment-scarce environments are unknown.

4.3 Effects of Sand Extraction on Bedforms and Fauna

Compared to the timescale associated to tidal sandbanks, sand extraction introduces a significantly faster morphological timescale of years to tens of years. Even faster is the system response of both smaller-scale bedforms and fauna after sand extraction. In these responses, we distinguish between local responses within the sand extraction pit itself and a distal response due to movement of sediment away from the pit.

In terms of local response, Bonne (2010) sampled the fauna from the depression in the Kwinte Bank a year after the region was closed for extraction to examine the short-term recovery. Bonne (2010) found that the macrobenthos density and species richness were similar over the central part of the Kwinte and Middelkerke Bank. Spatial variation was found in the depression, but not significantly different considering the wide range of species assemblages found in the tidal sandbanks of the BCS. Locally, the benthic fauna has adjusted to the sand extraction on the Kwinte Bank. Similar conclusions are drawn by Lopez Lopez et al. (2025), who note that physical and biological recovery commences directly after extraction. They analysed field data from the Buiten Ratel ranging from 2013-2023 and from the Thornthon bank from 2019-2023. They note that full morphological recovery (infill) is not observed, bedform and biological recovery are driven by local sediment reorganisation and colonisation by opportunistic species. At Buiten Ratel, small-scale seabed features like sand ripples gradually recover and macrobenthos communities return to reference conditions over 4 to 8 years (Lopez Lopez et al., 2025).

Van Lancker et al. (2024) highlight the importance of the distal response to sand extraction. As will be further examined in Chapter 5, the troughs between sandbanks on the BCS are often composed of rough gravel beds or exposed clay layers. These gravel beds are part of the broad habitat type (BHT) coarse sediments and have the potential to host rich biodiversity (Van Lancker et al., 2024). These are subject to indirect loss by (1) smothering and/or porefilling due to a veneer of silt or fine sand, impacting biogeochemical processes; and (2) sandification or burial of sand that leads to physical habitat loss of the BHT. Hence, predicting where the fine particles settle after sand extraction is critical in areas with gravel beds and richer biodiversity. In regions with high gravel biodiversity where no sand was present in 2006-2007, a field campaign showed significant coverage of an 8-10 cm sand layer in 2019 (Van Lancker et al., 2020). Note that just a few centimetres of burial is sufficient for intense mortification of macrobenthic species (Hendrick et al., 2016).

Chapter 5

Sediment Scarcity

In this chapter, we further explain the topic of sediment scarcity as a worldwide problem, and highlight the connection to the Belgian Continental shelf. Finally, we introduce several methods to take sediment scarcity into account for morphological models.

5.1 Sand as an Important and Scarce Resource

Sand is the second-most used raw resource on earth, after water (Vander Velpen et al., 2022). Annually, 40 to 50 billion tons (40 to $50 \cdot 10^{12}$ kg) of sand is used, which translates to 18 kg per person per day on average for construction, industries and coastal protection (Peduzzi, 2014). This demand is only increasing, from 9.6 in 1970 to 45.3 billion tons in 2020. In many parts of the world, the available sand is considered a scarce resource (Torres et al., 2021). However, as relatively little data is available, it is unclear if sand demand exceeds supply globally. Marine and river sand are often relatively easily accessible. This makes them a common-pool resource, where it appears to be abundant and access can only be limited with large costs. In turn, these kinds of resources are prone to overexploitation or degradation by selfish acts. Illegal sand extraction causes a variety of problems: ecosystem disruption, shoreline erosion and destabilisation, salt intrusion, social and political conflicts, and spreading of diseases (Torres et al., 2017). Illegal trade and extraction increase the issue of sand scarcity even further.

The relation of sediment scarcity to marine sand extraction is evident. However, there are currently no global policies or guidelines available that indicate how sand extraction should be done sustainably. Some countries have banned sand export, while others lack legislation or monitoring altogether. Development of a global policy will require detailed knowledge of how much sand is used locally and globally and how much of this sand is replenished through natural processes (Torres et al., 2017). In response, *Marine Sand Watch* has been set up by the United Nations Environmental Program (UNEP). It aims to identify dredging activities and provide estimates of dredged sediment volumes using AIS data (inspired by *Global Fishing Watch*). The UNEP considers sand a strategic material (UNEP, 2023) and urges to increase scientific and technical knowledge that supports policy making and provides suggestions towards environmentally friendly sand extraction.

5.2 Sediment Scarcity in the Belgian Continental Shelf

Sediment is abundant on most parts of the NCS, and the thickness of the erodible sediment layer is large compared to the typical sandbank height. This is not the case for the BCS, where the freely available sediment is limited. Geologically speaking, we refer to these types of sediment as quaternary deposits,

which are prone to erosion. Alternatively, tertiary deposits are older and are generally more resistant to erosion. Freely moving sand at the top of the seabed, and the main component of tidal sandbanks is a quaternary geological feature on top of the non-erodible tertiary layer. On the BCS, tertiary strata are locally exposed at the seabed together with (harder to erode) coarse quaternary sediment (Le Bot et al., 2003). For example, no Quaternary deposits are found in the troughs around the Goote Bank, and around the Hinder Bank the thin Quaternary cover often consists of more (coarser) gravel. Overall, the thickness of the Quaternary is between 0 and 10 m (Le Bot et al., 2005), and less than 2.5 m in most regions between the sandbanks (Deleu & Van Lancker, 2007; Van Lancker et al., 2019). As there is no distinct shelf break on the BCS, sediment cannot accumulate and is thus recycled and distributed on the continental shelf, creating this thin layer of sediment (Hademenos et al., 2019). This sediment scarcity may not apply to all grain size classes but might vary between grain size classes. On the BCS, medium to coarse sand is relatively depleted, while other classes, such as fine sand, are still abundantly available (Van Lancker et al., 2019). Continuing the current-day dredging activities means the Belgian coarse to medium sand will be exhausted within the next 80 years. Also, permanent sandification of the gravel beds as a consequence of sediment extraction is a topic of concern, as it might damage existing macrobenthic species communities.

5.3 Influence of Sediment Scarcity on Bedforms

The influence of sediment scarcity on bedform development has been considered before. Experimental data is available for the smaller bedforms (dunes and tidal sandwaves), but is unavailable for tidal sandbanks. Using morphological models, it has only been studied recently: for ripples (Blondeaux et al., 2016), river dunes (Porcile et al., 2023), tidal sandwaves (Nnafie et al., 2023) and tidal sandbanks (Van Veelen et al., 2024). An overview of the influence of sediment scarcity on these different bedforms is given in Figure 5.1. Note that Van Veelen et al. (2024) use a 1DH model, focussing on cross-sectional dynamics, and the response in along-crest direction is still unknown.

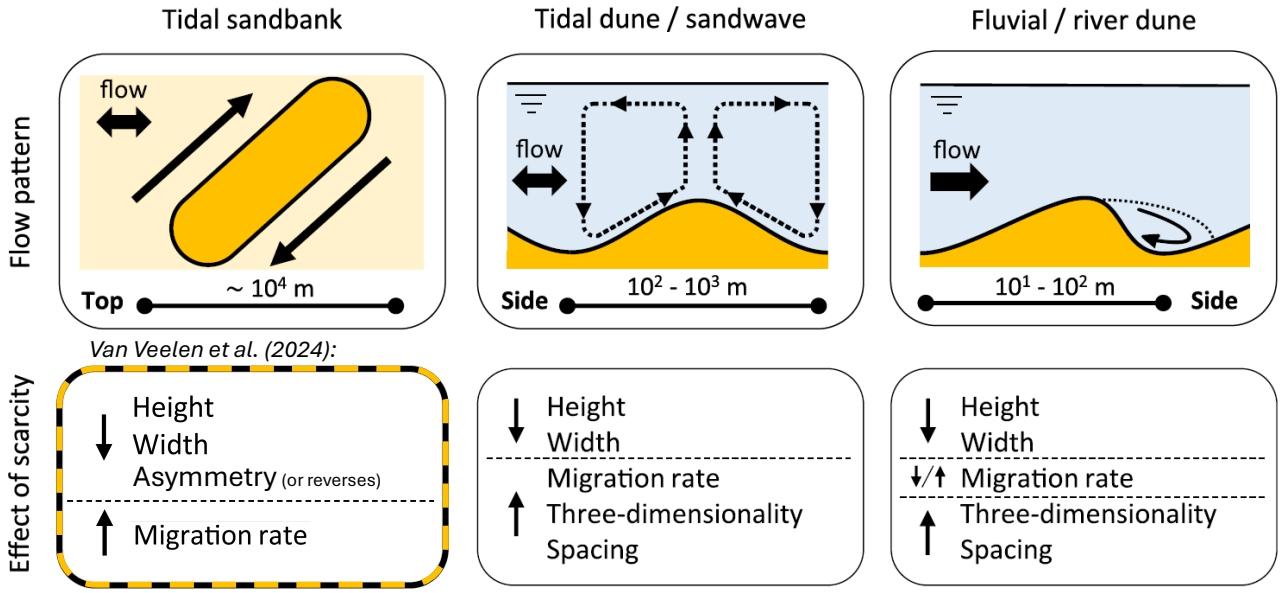

Figure 5.1: Influence of sediment scarcity on morphodynamic characteristics of different bedforms: tidal sandbanks, tidal sandwaves and river dunes. Figure adapted from Van Veelen et al. (2024), supplemented with outcomes of that respective research in the bottom left. See Van Veelen et al. (2024) for specific references on each bedform type.

For smaller bedforms, both flume experiments and numerical models have been performed to determine the influence of sediment scarcity on morphodynamic evolution on bedforms. This is usually done using a non-erodible flat bottom beneath a layer of mobile sediment. For tidal sand waves and river dunes, the height and width decrease with limited sediment, whereas the migration rate, three-dimensionality and crest-to-crest spacing increase (Nnafie et al., 2023; Porcile et al., 2023).

Due to the large temporal and spatial scale, no experimental data are available on the influence of scarcity on tidal sandbanks. In an idealised model, Van Veelen et al. (2024) show that sediment scarcity decreases the height, asymmetry and cross-sectional width of tidal sandbanks, whereas the migration rate is larger compared to the situation with an unbounded availability of sediment.

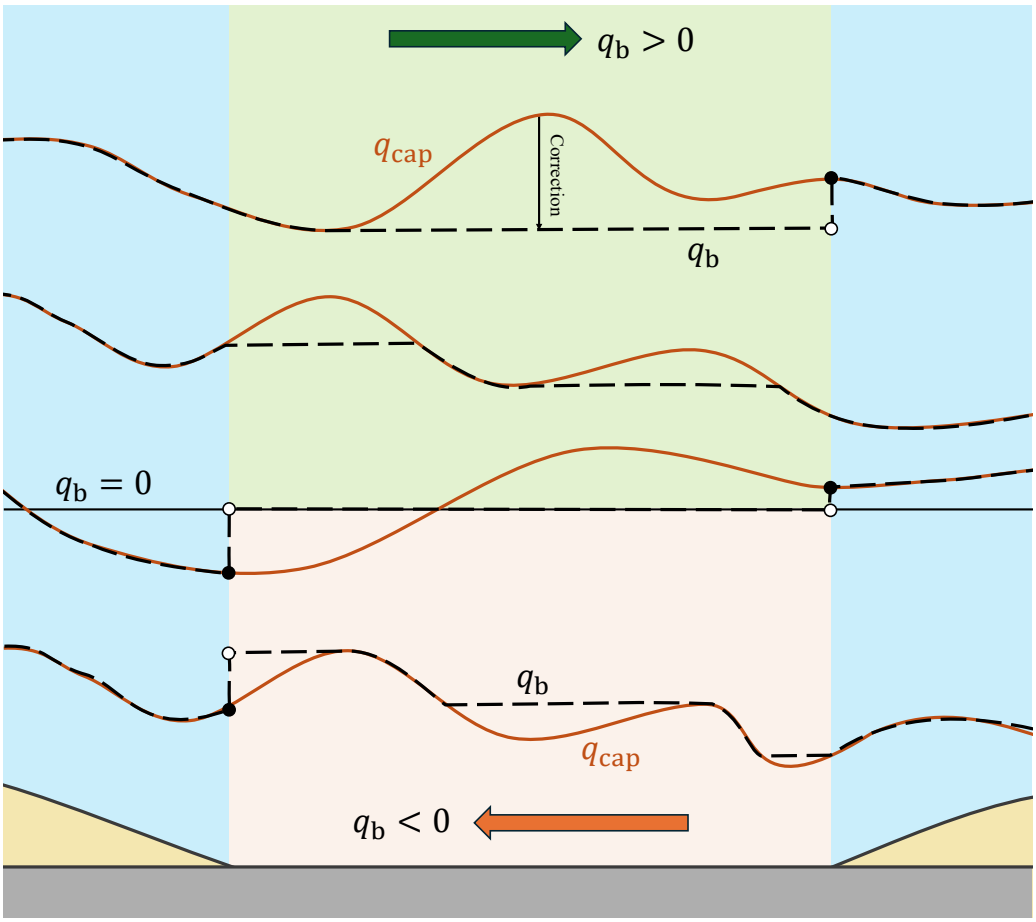

Figure 5.2: Schematisation of correction of the sediment transport capacity q_{cap} towards the physical transport rate. q_b. Grey visualises the non-erodible layer. Blue regions where there is still sand available. Green and orange the spatial extent where the non-erodible layer is exposed and where the sediment transport rate is rightward or leftward directed, respectively.

5.4 Bedload Transport over Non-Erodible Layers

First, we discuss how the bedload transport should behave physically over non-erodible layers. When the non-erodible layer is completely exposed, no erosion can take place and it follows from the Exner equation that $\nabla \cdot \boldsymbol{q}_b \leq 0$. Locally, this can be interpreted as the correction

$$\frac{\partial q_{b,x}}{\partial x} \leftarrow \min\left(\frac{\partial q_{b,x}}{\partial x}, 0\right) \tag{5.1}$$

for one dimension, as described by Blondeaux et al. (2016). We note that this can be implemented globally for the bedload sediment transport rate $\boldsymbol{q}_\mathrm{b}$ by distinguishing between a bedload sediment transport capacity q_cap and the true physical local sediment transport q_b. The latter is derived from the first throughout the region of exposed non-erodible layer. Figure 5.2 displays several (fictional) transport capacity intensities over a non-erodible layer in a one-dimensional model, and shows how this correction takes place. On top of the non-erodible layer, the magnitude local true sediment transport cannot exceed the nearest upwind local magnitude minimum. In two horizontal dimensions, this can be done by correction along the streamlines.

5.5 Modelling of Sediment Scarcity

The physics of Section 5.4 do not directly provide an exact modeling method. Note that these rules are only valid when the non-erodible layer is exposed exactly. However, with most numerical time-steppers, the moment this happens might overshoot. In this section, we will highlight the existence of different model formulations and how they deal with this issue (see for example Rulot et al., 2012), also discuss both physical and numerical difficulties with each.

5.5.1 Adapting Transport based on Divergence Rule

The rules of Section 5.4 are also described in similar fashion by Blondeaux et al. (2016) and Porcile et al. (2023), who appear to solve this iteratively along the direction of sediment transport, rather than the global approach highlighted with Figure 5.2.

Even when the overall transport capacity is adapted, challenges still arise at the transition region between the non-erodible bed and the movable sediment. First, this method can result in discontinuous jumps in $\boldsymbol{q}$ at the downwind transition zone (see Figure 5.2). Blondeaux et al. (2016) and Porcile et al. (2023) also note that this method introduces strong nonlinearities, meaning that the temporal evolution of the bed can only be done using numerical techniques. Furthermore, the sudden change in bed slope causes small-scale spurious oscillations as a result of the Gibbs' effect. Porcile et al. (2023) solve this in the numerical time-stepping procedure, where the model forces the bed elevation to never drop below the level of the substratum by applying a filtering procedure that removes these small-scale oscillations.

5.5.2 Struiksma Method

An alternative is known as the Struiksma method, where the sediment transport rate is limited in regions above and near exposed non-erodible layers (Struiksma, 1999). In existing numerical morphological model software, such as Delft3D, this is implemented by setting sediment transport to zero on top of the non-erodible layer (e.g. Damveld et al. (2021) and Nnafie et al. (2023)). This does not precisely model the physics accurately; only erosion can not take place, while sediment transport can still occur above a non-erodible layer when exposed. For some sediment transport patterns, such as the second from the bottom in Figure 5.2, it is the correct approach. However, it is generally an unphysical approach, as sediment will accumulate at the transition from mobile sand to the exposed non-erodible layer.

5.5.3 Limiting Erosion using Suspended Load

To retain a physical representativeness and not rely on numerical means, Van Veelen et al. (2024) models sediment transport as suspended load only. Here, the erosion rate is modelled by an entrainment concentration, which can be limited locally on the non-erodible bed. To remove discontinuities, a vertical transition boundary layer is implemented that smoothly introduces this non-erodibility. The

obtained sandbank shapes are representative of sandbanks in sediment-scarce environments, but this model does not capture the dominant bedload sediment transport mode.

5.5.4 Iterative Prediction Correction

Prediction-correction approaches provide a numerical procedure to deal with non-erodible layers (e.g. Rulot et al., 2012; Corestein et al., 2014). In the case of Rulot et al. (2012), the bed level is updated as if no non-erodible layer is present. Then, if this predicted bottom is below the rigid bed, the outward fluxes from each grid cell are corrected to ensure that the final bed level is exactly at the non-erodible layer. This procedure may in turn induce other non-physical configurations in neighbouring cells, so these steps are repeated iteratively and eventually leads to a configuration in which the levels are all in their physical range (Rulot et al., 2012). The approach of Corestein et al. (2014) is similar, but the prediction is made using outgoing fluxes only, and it is argued that no iterative approach is required.

These methods rely on numerical approaches, rather than a physical interpretation. Another issue with all methods above is dealing with the down-slope dispersion term (II in Equation (3.7)). When only updating the bed level in grid cells where the non-erodibility would be violated, the bed slope to neighbouring cells changes. This then decreases down-slope dispersion, meaning that the erosion would be larger than corrected to. Note that the influence of these errors is likely minor and will converge with smaller spatial and temporal steps.

5.5.5 Optimisation Problem

The above argues that the sediment transport rate should be updated globally for all bed-load fluxes. A method for this is introduced by Rulot et al. (2012) using an optimisation method. They argue that in every cell i the bedload transport capacity q_{cap} should be modified by a correction factor α_i to obtain the true local bedload transport

$$q_{\text{b},i} = \alpha_i q_{\text{cap},i}. \tag{5.2}$$

The optimal set of values of α_i should then ensure that the bed level does not violate the non-erodibility, meaning $z_{b,i} \geq z_{b,i}^{min}$, while making the change α_i from capacity to true bedload as minimal as possible. Rulot et al. (2012) compares a linear optimisation problem to a quadratic problem and shows that only a more restrictive linear optimisation problem

$$\begin{aligned} &\min \sum_i -\alpha_i \\ &\text{s.t. } 0 \leq \alpha_i \leq 1 \\ &\quad z_{\text{b},i} \geq z_{\text{b},i}^{min} \end{aligned} \tag{5.3}$$

properly reflects the actual physical behaviour of the morphodynamic system and provides a global solution procedure. The downside is that it might be more computationally expensive.

Chapter 6

Conclusions

In this final chapter, we summarise the answers to the four formulated literature research questions that were introduced in Chapter 1.

Q1 *What are tidal sandbanks and what is their relation to the Belgian Continental Shelf?*

Tidal sandbanks are large bedforms that evolve in shelf seas with a sandy bed when tidal flow velocities are sufficiently large. They form due to a positive feedback loop between hydrodynamics and morphodynamics, causing sediment transport patterns directed towards the crest due to bed friction and Coriolis effects. Tidal sandbanks are present throughout the entire Belgian Continental Shelf (BCS). They form the main locations where marine sand extraction takes place due to their shallow depth above the crest, are important ecological areas, and provide potential windfarm locations.

Q2 *What are the governing physical processes of tidal sandbank dynamics, and how can this be modelled?*

Tidal sandbanks form due to a residual cyclonic flow that causes up-crest movement of sediment. The depth-averaged shallow water equations are sufficient to capture the associated hydrodynamic processes, modelling the conservation of mass and momentum and implementing Coriolis effects, friction and free surface response. We distinguish between several model types. Due to the specific problem investigated, we are especially interested in nonlinear idealised models. These model the finite-height behaviour of tidal sandbanks and allow for determination of the relative contribution of several physical procceses, while retaining computational efficiency.

Q3 *How do large-scale sand extractions influence hydrodynamic and morphodynamic processes?*

The morphodynamic evolution of sandpits is analagous to tidal sandbanks and the sandpits can trigger the development of adjacent large-scale humps in a much larger area surrounding the sandpit, and is slow on a decadal scale. The impact on the local and distal hydrodynamics is rather limited, but continuous extraction activities are likely to make the whole system more vulnerable. Sand extraction pits on the BCS do not recover to the pre-extraction bathymetry, likely caused by a limited supply of sediment, but recovery of ripples and macrobenthic species is observed relatively quickly (within 10 years).

Q4 *How does sediment scarcity influence bedform development and how can this be modelled?*

The total amount of useful sediment on the BCS is limited and will be depleted within 80 years if the current sand extraction intensity continues. Generally, sediment scarcity decreases all spatial dimensions of bedforms while increasing their migration rate. For tidal sandbanks, asymmetry can reverse. Several methods exist to take sediment scarcity into account for morphodynamic modelling. Most of these methods lack physical representativeness but increase computational efficiency.

Bibliography

Amoudry, L. O., & Souza, A. J. (2011). Deterministic coastal morphological and sediment transport modeling: A review and discussion. *Reviews of Geophysics*, *49*(2). https://doi.org/10.1029/2010RG000341

Atalah, J., Fitch, J., Coughlan, J., Chopelet, J., Coscia, I., & Farrell, E. (2013). Diversity of demersal and megafaunal assemblages inhabiting sandbanks of the irish sea. *Marine Biodiversity*, *43*, 121–132. https://doi.org/10.1007/s12526-012-0139-y

Besio, G., Blondeaux, P., & Vittori, G. (2006). On the formation of sand waves and sand banks. *Journal of Fluid Mechanics*, *557*, 1–27. https://doi.org/10.1017/S0022112006009256

Blondeaux, P., & Vittori, G. (2005). Flow and sediment transport induced by tide propagation: 2. the wavy bottom case. *Journal of Geophysical Research: Oceans*, *110*(C8). https://doi.org/10.1029/2004JC002545

Blondeaux, P., De Swart, H. E., & Vittori, G. (2009). Long bed waves in tidal seas: An idealized model. *Journal of fluid mechanics*, *636*, 485–495. https://doi.org/10.1017/S0022112009990887

Blondeaux, P., Vittori, G., & Mazzuoli, M. (2016). Pattern formation in a thin layer of sediment. *Marine Geology*, *376*, 39–50. https://doi.org/10.1016/j.margeo.2016.03.011

Bonne, W. M. (2010). Macrobenthos characteristics and distribution, following intensive sand extraction from a subtidal sandbank. *Journal of Coastal Research*, 141–150. https://doi.org/10.2112/SI51-0.13.1

Brière, C., Roos, P. C., Garel, E., & Hulscher, S. J. M. H. (2010). Modelling the morphodynamics of the kwinte bank, subject to sand extraction. *Journal of coastal research*, 117–126. https://doi.org/10.2112/SI51-011.1

Calvete, D., Falqués, A., De Swart, H. E., & Walgreen, M. (2001). Modelling the formation of shoreface-connected sand ridges on storm-dominated inner shelves. *Journal of Fluid Mechanics*, *441*, 169–193. https://doi.org/10.1017/S0022112001004815

Campmans, G. H. P., Roos, P. C., De Vriend, H. J., & Hulscher, S. J. M. H. (2017). Modeling the influence of storms on sand wave formation: A linear stability approach. *Continental Shelf Research*, *137*, 103–116. https://doi.org/10.1016/j.csr.2017.02.002

Caston, V. N. D. (1972). Linear sand banks in the southern north sea. *Sedimentology*, *18*(1-2), 63–78. https://doi.org/10.1111/j.1365-3091.1972.tb00003.x

Corestein, G., Bladé, E., & Niñerola, D. (2014). Modelling bedload transport for mixed flows in presence of a non-erodible bed layer. *River Flow*, 1611–1618. https://doi.org/10.1201/b17133

Damveld, J. H., Borsje, B. W., Roos, P. C., & Hulscher, S. J. M. H. (2020). Horizontal and vertical sediment sorting in tidal sand waves: Modeling the finite-amplitude stage. *Journal of Geophysical Research: Earth Surface*, *125*(10), e2019JF005430. https://doi.org/10.1029/2019JF005430

Damveld, J. H., Porcile, G., Blondeaux, P., & Roos, P. C. (2021). Nonlinear dynamics of sand waves in sediment scarce environments. *EGU General Assembly 2021: vEGU21: Gather Online*. https://doi.org/10.5194/egusphere-egu21-16019

Damveld, J. H., Roos, P. C., Borsje, B. W., & Hulscher, S. J. M. H. (2019). Modelling the two-way coupling of tidal sand waves and benthic organisms: A linear stability approach. *Environmental fluid mechanics*, *19*(5), 1073–1103. https://doi.org/10.1007/s10652-019-09673-1

de Swart, H. E., & Yuan, B. (2019). Dynamics of offshore tidal sand ridges, a review. *Environmental Fluid Mechanics*, *19*(5), 1047–1071. https://doi.org/10.1007/s10652-018-9630-8

De Backer, A., Breine, N., Hans, H., Ellen, P., Jan, R., Van Hoey Gert, W. J., & Kris, H. (2017). Ecological assessment of intense aggregate dredging activity on the Belgian part of the North Sea. *Belgian marine sand: a scarce resource?*, 47. https://www.researchgate.net/publication/317958430_Ecological_assessment_of_intense_aggregate_dredging_activity_on_the_Belgian_part_of_the_North_Sea

De Hauwere, N. (2023). Maritime boundaries geodatabase: Maritime boundaries and exclusive economic zones (200nm), version 12 [Accessed on 06/03/2025 online]. https://doi.org/10.14284/632

Degrendele, K., Roche, M., Schotte, P., Van Lancker, V. R. M., Bellec, V., & Bonne, W. (2010). Morphological evolution of the kwinte bank central depression before and after the cessation of aggregate extraction. *Journal of Coastal Research*. https://doi.org/10.2307/40928820

Deleu, S., & Van Lancker, V. R. M. (2007). Geological setting of gravel occurrences on the belgian part of the north sea. *Management, Research and Budgeting of Aggregates in Shelf Seas Related to End-Users (Marebasse)*, 101–115.

Deleu, S., Van Lancker, V. R. M., Van den Eynde, D., & Moerkerke, G. (2004). Morphodynamic evolution of the kink of an offshore tidal sandbank: the Westhinder Bank (Southern North Sea). *Continental Shelf Research*, *24*(15), 1587–1610. https://doi.org/10.1016/j.csr.2004.07.001

Dodd, N., Blondeaux, P., Calvete, D., De Swart, H. E., Falqués, A., Hulscher, S. J. M. H., Różyński, G., & Vittori, G. (2003). Understanding coastal morphodynamics using stability methods. *Journal of coastal research*, 849–865. https://www.jstor.org/stable/4299224

Dujardin, A., Houthuys, R., Nnafie, A., Röbke, B., van der Werf, J., de Swart, H., & Biernaux, V. (2023). Mozes–research on the morphological interaction between the sea bottom and the belgian coastline.

Durinck, R., & Casteleyn, K. (2017). Update environmental impact report for the extraction of marine aggregates in control zones 1, 2 and 3 in the Belgian part of the North Sea. *Belgian marine sand: a scarce resource?*, 105.

Dyer, K. R. (1986). Coastal and estuarine sediment dynamics. *John Wiley*.

Dyer, K. R., & Huntley, D. A. (1999). The origin, classification and modelling of sand banks and ridges. *Continental Shelf Research*, *19*(10), 1285–1330. https://doi.org/10.1016/S0278-4343(99)00028-X

Eisma, D., Jansen, J., van Weering, T. C., et al. (1979). Sea-floor morphology and recent sediment movement in the north sea. In *The quaternary history of the north sea* (pp. 217–231, Vol. 2). Acta Universitatis Upsaliensis Uppsala.

Fredsoe, J., & Deigaard, R. (1992). *Mechanics of coastal sediment transport* (Vol. 3). World scientific publishing company.

Geerts, S. J., Röbke, B., & Geurts, B. J. (2023). Influence of sfcr on longshore sediment transport at the belgian coast. *NCK-days 2023*. https://www.nck-web.org/boa-2023/603-influence-of-sfcr-on-longshore-sediment-transport-at-the-belgian-coast

González, M., Medina, R., Espejo, A., Tintoré, J., Martin, D., & Orfila, A. (2010). Morphodynamic evolution of dredged sandpits. *Journal of Coastal Research*, *26*(3), 485–502. https://doi.org/10.2112/08-1034.1

Hademenos, V., Stafleu, J., Missiaen, T., Kint, L., & Van Lancker, V. R. M. (2019). 3d subsurface characterisation of the belgian continental shelf: A new voxel modelling approach. *Netherlands Journal of Geosciences*, *98*, e1. https://doi.org/10.1017/njg.2018.18

Hendrick, V. J., Hutchison, Z. L., & Last, K. S. (2016). Sediment burial intolerance of marine macroinvertebrates. *PloS one*, *11*(2), e0149114. https://doi.org/10.1371/journal.pone.0149114

Hulscher, S. J. M. H. (1996). Tidal-induced large-scale regular bed form patterns in a three-dimensional shallow water model. *Journal of geophysical research: Oceans*, *101*(C9), 20727–20744. https://doi.org/10.1029/96JC01662

Hulscher, S. J. M. H., de Swart, H. E., & de Vriend, H. J. (1993). The generation of offshore tidal sand banks and sand waves. *Continental shelf research*, *13*(11), 1183–1204. https://doi.org/10.1016/0278-4343(93)90048-3

Huthnance, J. (1973). Tidal current asymmetries over the norfolk sandbanks. *Estuarine and Coastal Marine Science*, *1*(1), 89–99. https://doi.org/10.1016/0302-3524(73)90061-3

Huthnance, J. M. (1982). On one mechanism forming linear sand banks. *Estuarine, Coastal and Shelf Science*, *14*(1), 79–99. https://doi.org/10.1016/S0302-3524(82)80068-6

Idier, D., & Astruc, D. (2003). Analytical and numerical modeling of sandbanks dynamics. *Journal of geophysical research: Oceans*, *108*(C3). https://doi.org/10.1029/2001JC001205

Idier, D., van Der Veen, H., & Hulscher, S. J. M. H. (2009). Grain size dependency in sandbank modeling for the case of uniform sediment. *Journal of Geophysical Research: Earth Surface*, *114*(F3). https://doi.org/10.1029/2008JF001140

Kint, L., Barette, F., Degrendele, K., Roche, M., & Van Lancker, V. R. M. (2023). Sediment variability in intermittently extracted sandbanks in the belgian part of the north sea. *Frontiers in Earth Science*, *11*, 1154564. https://doi.org/10.3389/feart.2023.1154564

Knaapen, M. A. F. (2009). Sandbank occurrence on the dutch continental shelf in the north sea. *Geo-marine letters*, *29*, 17–24. https://doi.org/10.1007/s00367-008-0105-7

Komarova, N. L., & Newell, A. C. (2000). Nonlinear dynamics of sand banks and sand waves. *Journal of Fluid Mechanics*, *415*, 285–321. https://doi.org/10.1017/S0022112000008855

Le Bot, S., Van Lancker, V. R. M., Deleu, S., De Batist, M., & Henriet, J. P. (2003). Tertiary and quaternary geology of the belgian continental shelf.

Le Bot, S., Van Lancker, V. R. M., Deleu, S., De Batist, M., Henriet, J., & Haegeman, W. (2005). Geological characteristics and geotechnical properties of eocene and quaternary deposits on the belgian continental shelf: Synthesis in the context of offshore wind farming. *Netherlands Journal of Geosciences*, *84*(2), 147–160. https://doi.org/10.1017/S0016774600023027

Leenders, S., Damveld, J. H., Schouten, J., Hoekstra, R., Roetert, T. J., & Borsje, B. W. (2021). Numerical modelling of the migration direction of tidal sand waves over sand banks. *Coastal engineering*, *163*, 103790. https://doi.org/10.1016/j.coastaleng.2020.103790

Lopez Lopez, L., Degrendele, K., Roche, M., Barette, F., Van Lancker, V. R. M., Terseleer, N., & De Backer, A. (2025). Macrobenthos and morpho-sedimentary recovery dynamics in areas following aggregate extraction cessation. *Marine Pollution Bulletin*, *218*, 118184. https://doi.org/10.1016/j.marpolbul.2025.118184

McCarron, C. J., Van Landeghem, K. J. J., Baas, J. H., Amoudry, L. O., & Malarkey, J. (2019). The hiding-exposure effect revisited: A method to calculate the mobility of bimodal sediment mixtures. *Marine Geology*, *410*, 22–31. https://doi.org/10.1016/j.margeo.2018.12.001

Nnafie, A., Krabbendam, J. M., & de Swart, H. E. (2023). Consequences of limited sediment supply for long-term evolution of offshore tidal sand waves, a 3d model perspective. *Marine Geology*, *464*, 107148. https://doi.org/10.1016/j.margeo.2023.107148

Nnafie, A., Wolf, T. B. J., & de Swart, H. E. (2020). Tidal sand ridges on the shelf: A numerical study of their natural morphodynamic evolution and response to interventions. *Continental Shelf Research*, *205*, 104195. https://doi.org/10.1016/j.csr.2020.104195

Off, T. (1963). Rhythmic linear sand bodies caused by tidal currents. *AAPG bulletin*, *47*(2), 324–341. https://doi.org/10.1306/BC743989-16BE-11D7-8645000102C1865D

Parker, G. (1978). Self-formed straight rivers with equilibrium banks and mobile bed. part 1. the sand-silt river. *Journal of Fluid Mechanics*, *89*(1), 109–125. https://doi.org/10.1017/S0022112078002499

Peduzzi, P. (2014). Sand, rarer than one thinks. *Environmental Development*, *11*(208-218), 682. https://doi.org/10.1016/j.envdev.2014.04.001

Ploeg, W. (2024). *Modelling the interaction among sand extraction, sediment composition, benthic organisms and sand wave dynamics* (tech. rep.) (CEM research report 2024R-001/WEM-001).

Porcile, G., Damveld, J. H., Roos, P. C., Blondeaux, P., & Colombini, M. (2023). Modeling the genesis of sand-starved dunes in steady currents. *Journal of Geophysical Research: Earth Surface*, *128*(1), e2022JF006796. https://doi.org/10.1029/2022JF006796

Ribberink, J. S. (1987). *Mathematical modelling of one-dimensional morphological changes in rivers with non-uniform sediment*. Citeseer.

Roche, M., Degrendele, K., Vandenreyken, H., & Schotte, P. (2017). Multi time and space scale monitoring of the sand extraction and its impact on the seabed by coupling ems data and mbes measurements. *Belgian marine sand: a scarce resource*, *7*, 164.

Roos, P. C., & Hulscher, S. J. M. H. (2003). Large-scale seabed dynamics in offshore morphology: Modeling human intervention. *Reviews of geophysics*, *41*(2). https://doi.org/10.1029/2002RG000120

Roos, P. C., Hulscher, S. J. M. H., & de Vriend, H. J. (2008). Modelling the morphodynamic impact of offshore sandpit geometries. *Coastal engineering*, *55*(9), 704–715. https://doi.org/10.1016/j.coastaleng.2008.02.019

Roos, P. C., Hulscher, S. J. M. H., Knaapen, M. A. F., & Van Damme, R. M. J. (2004). The cross-sectional shape of tidal sandbanks: Modeling and observations. *Journal of Geophysical Research: Earth Surface*, *109*(F2). https://doi.org/10.1029/2003JF000070

Roos, P. C., Wemmenhove, R., Hulscher, S. J. M. H., Hoeijmakers, H. W. M., & Kruyt, N. P. (2007). Modeling the effect of nonuniform sediment on the dynamics of offshore tidal sandbanks. *Journal of Geophysical Research: Earth Surface*, *112*(F2). https://doi.org/10.1029/2005JF000376

Rulot, F., Dewals, B. J., Erpicum, S., Archambeau, P., & Pirotton, M. (2012). Modelling sediment transport over partially non-erodible bottoms. *International Journal for Numerical Methods in Fluids*, *70*(2), 186–199.

Schuttelaars, H. M., & De Swart, H. E. (1996). An idealized long-term morphodynamic model of a tidal embayment. *EUROPEAN JOURNAL OF MECHANICS SERIES B FLUIDS*, *15*, 55–80.

Struiksma, N. (1999). Mathematical modelling of bedload transport over non-erodible layers. *Proceedings IAHR Symp. River Coastal and Estuarine Morphodynamics, Genova*, *1*, 89–98.

Talmon, A. M., Struiksma, N., & Van Mierlo, M. C. L. M. (1995). Laboratory measurements of the direction of sediment transport on transverse alluvial-bed slopes. *Journal of hydraulic research*, *33*(4), 495–517. https://doi.org/10.1080/00221689509498657

Tambroni, N., & Blondeaux, P. (2008). Sand banks of finite amplitude. *Journal of Geophysical Research: Oceans*, *113*(C10). https://doi.org/10.1029/2007JC004658

Torres, A., Brandt, J., Lear, K., & Liu, J. (2017). A looming tragedy of the sand commons. *Science*, *357*(6355), 970–971. https://doi.org/10.1126/science.aao0503

Torres, A., Simoni, M. U., Keiding, J. K., Müller, D. B., zu Ermgassen, S. O., Liu, J., Jaeger, J. A., Winter, M., & Lambin, E. F. (2021). Sustainability of the global sand system in the anthropocene. *One Earth*, *4*(5), 639–650. https://doi.org/10.1016/j.oneear.2021.04.011

UNEP. (2023). Unep marine sand watch reveals massive extraction in the world's oceans [Published on 12 Feb 2025]. https://www.unep.org/news-and-stories/press-release/unep-marine-sand-watch-reveals-massive-extraction-worlds-oceans

Van den Eynde, D., Giardino, A., Portilla, J., Fettweis, M., Francken, F., & Monbaliu, J. (2010). Modelling the effects of sand extraction, on sediment transport due to tides, on the kwinte bank. *Journal of Coastal Research*, 101–116.

Van den Eynde, D., Verwaest, T., & Trouw, K. (2019). *The impact of sand extraction on the wave height near the belgian coast* (tech. rep.). RBINS-OD Nature and MUMM, Brussels.

Van Lancker, V. R. M., Baeye, M., Montereale Gavazzi, G., & Van den Eynde, D. (2020). Monitoring of the impact of the extraction of marine aggregates, in casu sand, in the zone of the Hinder Banks. Period 1/1 – 31/12 2019 and Synthesis of results 2016-2019. *Scientific Report*, 2011–2015. https://biblio.naturalsciences.be/library-1/rbins-staff-publications-2020/techreportreference.2020-12-16.3256121730

Van Lancker, V. R. M., Bonne, W. M. I., Garel, E., Degrendele, K., Roche, M., Van den Eynde, D., Bellec, V. K., Brière, C., Collins, M. B., & Velegrakis, A. F. (2010a). Recommendations for the sustainable exploitation of tidal sandbanks. *Journal of Coastal Research*, 151–164. http://www.jstor.org/stable/40928827

Van Lancker, V. R. M., Bonne, W. M. I., Velegrakis, A. F., & Collins, M. B. (2010b). Aggregate extraction from tidal sandbanks: Is dredging with nature an option? introduction. *Journal of Coastal Research*, 53–61. https://www.jstor.org/stable/40928818

Van Lancker, V. R. M., Francken, F., & Kint, L. (2024). Ratio hard substrate to soft sediment surfaces. https://odnature.naturalsciences.be/msfd_media/documents/D6-ANS-BE-BENT-H-S-2024-Ratio_hard_to_soft_sediments.pdf

Van Lancker, V. R. M., Frederic, F., Michel, K., Lars, K., Nathan, T., Rick, A., Van Heteren, S., Van Maanen, P.-P., Stafleu, J., Stam, J., Koen, D., & Marc, R. (2019). *Transnational and integrated long-term marine exploitation strategies* (tech. rep.). https://core.ac.uk/download/pdf/199195904.pdf

Van Lancker, V. R. M., Lauwaert, B., De Mol, L., Vandenreyken, H., De Backer, A., & Pirlet, H. (2022). Sand and gravel extraction. In *Dauwe, s. et al. (eds). knowledge guide coast and sea 2022 - compendium for coast and sea* (pp. 67–78). https://pureportal.ilvo.be/nl/publications/sand-and-gravel-extraction-2

Van Veelen, T. J., Roos, P. C., & Hulscher, S. J. M. H. (2024). Modeling the cross-sectional dynamics of tidal sandbanks in sediment-scarce conditions. *Journal of Geophysical Research: Earth Surface*, *129*(4), e2023JF007308. https://doi.org/10.1029/2023JF007308

Van Veelen, T. J., Roos, P. C., & Hulscher, S. J. M. H. (2018). Process-based modelling of bank-breaking mechanisms of tidal sandbanks. *Continental Shelf Research*, *167*, 139–152. https://doi.org/10.1016/j.csr.2018.04.007

Vander Velpen, A., Smeets, A., Torres, A., Matheson, A. B., Friot, D., Franks, D. M., Cuperus, G., Yusuf, H., van der Vegt, H., Selby, I., et al. (2022). Sand and sustainability: 10 strategic recommendations to avert a crisis. https://www.unep.org/resources/report/sand-and-sustainability-10-strategic-recommendations-avert-crisis

Verwaest, T., Dujardin, A., Nnafie, A., Houthuys, R., & Röbke, B. (2024). Mozes: Research on the morphological interaction between the sea bottom and the belgian coastline. *Coastal Engineering Proceedings*, (38), 21–21.

Walgreen, M., De Swart, H. E., & Calvete, D. (2003). Effect of grain size sorting on the formation of shoreface-connected sand ridges. *Journal of Geophysical Research: Oceans*, *108*(C3). https://doi.org/10.1029/2002JC001435

Wyns, L., Roche, M., Barette, F., Van Lancker, V. R. M., Degrendele, K., Hostens, K., & De Backer, A. (2021). Near-field changes in the seabed and associated macrobenthic communities due to marine aggregate extraction on tidal sandbanks: A spatially explicit bio-physical approach considering geological context and extraction regimes. *Continental Shelf Research*, *229*, 104546. https://doi.org/10.1016/j.csr.2021.104546

Yuan, B., de Swart, H. E., & Panadès, C. (2016). Sensitivity of growth characteristics of tidal sand ridges and long bed waves to formulations of bed shear stress, sand transport and tidal forcing: A numerical model study. *Continental Shelf Research*, *127*, 28–42. https://doi.org/10.1016/j.csr.2016.08.002

Yuan, B., de Swart, H. E., & Panadès, C. (2017). Modeling the finite-height behavior of offshore tidal sand ridges, a sensitivity study. *Continental Shelf Research*, *137*, 72–83. https://doi.org/10.1016/j.csr.2017.02.007

Yuan, B., & de Swart, H. E. (2017). Effect of sea level rise and tidal current variation on the long-term evolution of offshore tidal sand ridges. *Marine Geology*, *390*, 199–213. https://doi.org/10.1016/j.margeo.2017.07.005

Zimmerman, J. (1982). On the lorentz linearization of a quadratically damped forced oscillator. *Physics Letters A*, *89*(3), 123–124. https://doi.org/10.1016/0375-9601(82)90871-4